HELSINKI INSTITUTE OF PHYSICS INTERNAL REPORT SERIES

HIP-2016-03

Cosmological Constraints on Higgs Portal Dark Matter

Tommi Tenkanen

Helsinki Institute of Physics
University of Helsinki
Finland

ACADEMIC DISSERTATION

To be presented, with the permission of the Faculty of Science of the University of Helsinki, for public criticism in the auditorium E204 at Physicum, Gustaf Hällströmin katu 2A, Helsinki, on the 16th of December 2016 at 12 o'clock.

Helsinki 2016

ISBN 978-951-51-1265-1 (print)
ISBN 978-951-51-1266-8 (pdf)
ISSN 1455-0563
http://ethesis.helsinki.fi
Unigrafia
Helsinki 2016

Tähdistä meihin hiipii
epätoivon ja innostuksen kummallinen rajamaa

– A.W. Yrjänä, *Mechanema*

T. Tenkanen: Cosmological Constraints on Higgs Portal Dark Matter,
University of Helsinki, 2016, 65 pages,
Helsinki Institute of Physics, Internal Report Series, HIP-2016-03,
ISBN 978-951-51-1265-1,
ISSN 1455-0563.

Abstract

Cosmic inflation, an era of rapid expansion in the early universe, and dark matter, an unknown non-baryonic matter component exceeding the amount of the usual baryonic matter by a factor of five, are known to play an important role in describing the physics of the early universe and in explaining the contents of the universe we observe today. Yet the reason for the occurrence of inflation and for the production of dark matter, or their properties, are not known.

In this thesis we study the observational consequences of a class of particle physics models related to inflation and dark matter which are challenging to test by direct experiments, such as particle colliders, but which can be tested by cosmological and astrophysical observations. In particular, we concentrate on observational properties of self-interacting Higgs portal dark matter. Whenever a model contains scalar fields which are light and energetically subdominant during cosmic inflation, so-called 'spectator fields', they acquire large fluctuations which may leave observable imprints on the Cosmic Microwave Background radiation.

Carefully investigating the spectator field dynamics during cosmic inflation, we solve for typical initial conditions for post-inflationary dynamics and calculate the dark matter yield originating from non-thermal decay of spectator condensates. As a result, we find a novel connection between the energy scale of inflation and the dark matter abundance. We also study alternative thermal histories of hidden sector dark matter and demonstrate how the usual dark matter production mechanisms may not be sufficient to correctly describe the evolution of dark matter relic density from its generation to the present day.

We show that even if the coupling between the hidden and visible sectors is almost negligible, the scenario has observable consequences. Especially a positive observation of primordial tensor perturbations would immensely affect not only models of inflation but also very weakly coupled dark matter models, ruling out large portions of the otherwise viable parameter space. The derived bounds are generic to most weakly coupled portal models with light scalar fields, and qualitatively similar results are also expected to arise in other portal type extensions of the Standard Model of particle physics.

Acknowledgements

First and foremost, I thank Kari Enqvist, Sami Nurmi, and Kimmo Tuominen for supervision and guidance during my studies. All research projects presented in this thesis were inspired by one simple notion – that no thermalization happens if the interaction strength between two particle species is smaller than a certain threshold value – at the time we were completing my first research project. I find this an entrancing example of what making science is all about: making quantitative statements and trying to be as accurate as possible. This thesis is an example of how it can lead to taking new paths whose existence was unknown at the time the idea first came. For finding this path, I owe great gratitude to my aforementioned supervisors as they have always had time to discuss interesting new ideas with me.

I thank Ville Vaskonen, Kimmo Kainulainen, and Matti Heikinheimo for collaboration and discussions which have always been both insightful and enjoyable. Discussions with Chris Byrnes and Jussi Väliviita played an important role in conducting the research presented in this thesis, and I wish to thank them. The pre-examiners of this thesis, Martti Raidal and Arttu Rajantie, I thank for carefully reading the manuscript and providing useful comments. I also thank David Weir for proofreading the manuscript.

I acknowledge financial support from The Research Foundation of the University of Helsinki. I also thank Hannu Kurki-Suonio, Kari Rummukainen, Syksy Räsänen, the Alfred Kordelin foundation, the Emil Aaltonen foundation, the University of Helsinki Doctoral School in Natural Sciences and the Doctoral Programme in Particle Physics and Universe Sciences, and all my hosts for supporting my travels. They have been essential in initiating new research projects and collaborations.

The cheerful atmosphere at the Helsinki Institute of Physics has been invaluable in keeping up the good work also during the more challenging times. I am especially grateful to Keijo Kajantie and Aleksi Vuorinen for discussions, support, and tips they have given to me. My fellow doctoral students have made the atmosphere even more cheerful and entertaining. I sincerely thank all of you. Olli-Pekka Tikkanen deserves special thanks for friendship in the everlasting journey towards wisdom, beauty, and truth.

I thank all my colleagues in the boards of the Association of Doctoral Students at the University of Helsinki and the Finnish Physical Society, especially Sonja Trifuljesko, Julia von Boguslawski, Janne Ignatius, and Rami Vainio. The work done in both associations has kept me busy during my time as a doctoral student but has been great fun.

Finally, I wish to express my gratitude to my great family for continuous support, and to Sanni, without whom I would be nothing but dust and bones in a far away corner of the world.

List of Included Papers

This thesis is based on the following publications [1–3]:

I Inflationary Imprints on Dark Matter
S. Nurmi, T. Tenkanen and K. Tuominen
JCAP **1511**, 001 (2015)

II Isocurvature Constraints on Higgs Portal Couplings
K. Kainulainen, S. Nurmi, T. Tenkanen, K. Tuominen and V. Vaskonen
JCAP **1606**, 022 (2016)

III Observational Constraints on Decoupled Hidden Sectors
M. Heikinheimo, T. Tenkanen, K. Tuominen and V. Vaskonen
Phys. Rev. D **94**, 063506 (2016)

In all of the papers the authors are listed alphabetically according to particle physics convention.

The author's contribution

The author participated in writing of all articles. In paper **I** the author participated in all analytic calculations and carried out all numerical computations. In paper **II** the author participated in all analytic calculations and numerical computations. In paper **III** the author formulated the initial research problem, participated in its refinement throughout the work, and participated in all analytic calculations and numerical computations.

Contents

Chapter 1

Introduction

Cosmology is a discipline which studies the universe as a whole; it is the art of everything that exists. In the course of history of mankind it has led to a worldview, where instead of being at the center of the universe, we have been shown to live in a vast cosmos where our spatial location is in no particular way special.

The cosmological principle, being a guiding philosophy rather than a fundamental law of nature, states that we live in a spatially homogeneous and isotropic universe. Furthermore, at large scales the universe is expanding, and we know that at least the observable part of our universe is not infinitely old but was in a state of hot and dark plasma compressed into a tiny volume approximately 13.8 billion years ago. Ever since it has been expanding and cooling, evolving differently at different length scales towards the state we observe today [4–7].

It is likely that even before the so-called Hot Big Bang state in the very early universe there were events such as cosmic inflation [8–10], the primordial era of rapid expansion, but at the moment we do not know that for sure. Likewise, we are not at the end of the cosmic history. The expansion of the universe will continue, probably indefinitely [7], and eventually it will empty the universe we observe today.

The crucial point in scientific research is reaching conclusions based on observations and experiments. The above description can be claimed to be 'true' because it is based on observations of the large scale structure of the universe [11], the Cosmic Microwave Background [7], ratios of light elements [12], and many other things which, when tested, criticized, tested again, and finally glued together, form a coherent worldview which can be stated to be true to the best of our knowledge.

Yet there remain unsolved issues. They are related for example to the evolution, fundamental matter content, and the very beginning of our universe. This thesis concentrates on a combination of the latter two: on the nature of so-called dark matter and its role in the very early universe.

We study the observational consequences of a class of particle physics models which are challenging to test by direct Earth-bound experiments, such as particle colliders, but which can be tested through cosmological and astrophysical observations. Making predictions, deriving constraints for new models from what we already know, and utilizing observations at all scales within our reach are important to improve and sharpen our understanding of the universe we live in. This is what we intend to do

in this thesis.

In particular, the contribution of this thesis is to provide an example of an extension of the Standard Model of particle physics (SM) where new physics even with a tiny coupling to the SM can be constrained by carefully investigating their dynamics both during and after cosmic inflation. We hope this will not only provide information about this particular class of models but also motivate other studies to take the advantage of what we know about the physics of the early universe today.

The thesis is organized as follows. In Chapter 1 we give a brief introduction to the so-called ΛCDM cosmology, review the thermal history of our universe and the basis for cosmological perturbation theory and inflation, and discuss the main observations made of the physics of the very early universe. In Chapter 2 we concentrate on dark matter by presenting the current observational evidence for its existence and discussing different production mechanisms and observational properties of very weakly coupled particle dark matter. In Chapter 3 we focus on the phenomenology of scalar fields in a curved background, discussing their role during and after cosmic inflation. In Chapter 4 we discuss the observational need to extend the Standard Model of particle physics and present the Higgs portal model together with its defining principles and particle content. In Chapter 5 we discuss the evolution of different Higgs portal fields in the early universe and derive cosmological constraints on different properties of this class of models. Finally, we conclude with an outlook in Chapter 6.

1.1 Friedmann–Robertson–Walker universe

The general theory of relativity is defined by the Einstein-Hilbert action [5]

$$S = \int d^4x\sqrt{-g}\left(\frac{R}{16\pi G} + \mathcal{L}_{\rm mat}\right) \tag{1.1}$$

where g is the determinant of the metric tensor $g_{\mu\nu}$, R is the Ricci scalar, G is the Newton's gravitational constant and $\mathcal{L}_{\rm mat}$ denotes the Lagrangian density of the matter content of the universe.

Varying with respect to the metric $g_{\mu\nu}$ leads to the Einstein field equations

$$R_{\mu\nu} - \frac{1}{2}g_{\mu\nu}R = 8\pi G T_{\mu\nu}, \tag{1.2}$$

where $R_{\mu\nu}$ is the Ricci tensor and $T_{\mu\nu}$ is the energy-momentum tensor. The Einstein equations describe how the curvature of spacetime reacts to the presence of matter, and how in turn the matter content evolves in the presence of spacetime curvature. In this sense, Eq. (1.2) is the governing equation of cosmology.

Assuming a spatially homogeneous and isotropic universe, the spacetime metric takes the Robertson–Walker (RW) form [5, 6]

$$ds^2 = -dt^2 + a^2(t)\left(\frac{dr^2}{1-Kr^2} + r^2\left(d\theta^2 + \sin^2\theta d\phi^2\right)\right), \tag{1.3}$$

where $a(t)$ is a time-dependent scale factor and K a real-valued parameter which describes spatial curvature[1]. Models based upon this metric are called Friedmann–Robertson–Walker models.

The evolution of $a(t)$ is determined by the Friedmann equations

$$\left(\frac{\dot{a}}{a}\right)^2 + \frac{K}{a^2} = \frac{8\pi G}{3}\rho, \qquad \frac{\ddot{a}}{a} = -\frac{4\pi G}{3}(\rho + 3p), \tag{1.4}$$

which can be derived by inserting the metric (1.3) into the Einstein equation (1.2) and assuming the energy-momentum tensor takes the form of a perfect fluid, $T_{\mu\nu} = (\rho + p)U_\mu U_\nu + p g_{\mu\nu}$, where U_μ is the fluid four-velocity in comoving coordinates. Here ρ and p are, respectively, the energy density and pressure of the fluid.

Conservation of the energy-momentum tensor, $\nabla^\mu T_{\mu\nu} = 0$, implies

$$\frac{\dot{\rho}}{\rho} = -3(1+\omega)\frac{\dot{a}}{a}, \tag{1.5}$$

where $\omega \equiv p/\rho$ is the equation of state parameter of the fluid. There are three forms of cosmological fluids: matter (dust), radiation, and vacuum energy. Matter consists of nonrelativistic particles which have zero pressure, $\omega = 0$, and whose energy density, in case there are no interactions between different particle species, falls off in an expanding universe as $\rho_{\rm m} \propto a^{-3}$ by virtue of Eq. (1.5). Radiation may describe either actual electromagnetic radiation or massive particles moving at relativistic velocities, and its equation of state is $\omega = 1/3$. The energy density of radiation therefore falls off as $\rho_{\rm r} \propto a^{-4}$. Vacuum energy has an equation of state $\omega = -1$, and hence its energy density remains constant, $\rho_\Lambda \propto a^0$, as the universe expands.

Equations (1.4) and (1.5) can be written either in the above form or in terms of the Hubble parameter, $H \equiv \dot{a}/a$, which characterizes the rate of expansion of the universe. The measured value of the Hubble parameter at the present epoch[2] is $H_0 = (67.8 \pm 0.9)$ km/s/Mpc [7], which is sometimes written as $H_0 = 100h$ km/s/Mpc, where $h \approx 0.68$.

Defining the Hubble parameter allows us to write the Friedmann equation (1.4) as

$$\sum_i \Omega_i - 1 = \frac{K}{H^2 a^2}, \tag{1.6}$$

where $\Omega_i = \rho_i/\rho_c$ is the density parameter defined in terms of the critical density $\rho_c \equiv 3H_0^2/(8\pi G)$, and where the sum runs over all the different matter components of the universe. Recent measurements by the Planck satellite show that $\Omega_{\rm m} = 0.308 \pm 0.012$, $\Omega_{\rm r} \simeq 5 \times 10^{-5}$, $\Omega_\Lambda = 0.692 \pm 0.012$ [7]. The measured values of the matter density parameters show that out of all possible values the sum $\sum_i \Omega_i$ is very close to unity, implying that K is very close to zero and space is essentially flat. More accurately, Planck finds $|\Omega_K| \leq 0.005$ [7].

[1] Alternatively, the parameter K can be normalized such that $K = -1, 0,$ and 1 refer to an open, flat, or closed universe, respectively.

[2] It should be noted that there is more than a 2σ discrepancy in H_0 between local measurements and observations of the Cosmic Microwave Background radiation [13, 14] (see also [15]). The reason for this discrepancy has recently been studied in e.g. [16].

This scenario, where the spacetime metric is described by the flat RW form, (1.3) with $K = 0$, and the matter content of the universe consists mostly of non-relativistic matter and vacuum energy, is known as the ΛCDM model. Here CDM refers to cold dark matter, to be discussed first in Section 1.2.2 and then in more detail in Chapter 2. The ΛCDM model is also called the Standard Model of cosmology for its prevalent role in explaining the cosmological matter content and evolution of our universe [6, 7]. In the remainder of this Chapter we will discuss the cosmic evolution of the different components of the ΛCDM model.

1.2 Thermal history of the universe

The history of the universe is well understood down to the time of Big Bang Nucleosynthesis (BBN), which took place at $t \simeq 1s$. The BBN describes successfully how and in what ratios light atomic nuclei formed, and it is one of the cornerstones of modern cosmology [6]. Another cornerstone is the formation of the Cosmic Microwave Background radiation (CMB) at $t \simeq 4 \times 10^5 y$, when photons decoupled from atomic nuclei and the universe became transparent for the first time. Therefore, the CMB is the first light and can be described as the afterglow of the Hot Big Bang era.

The success of BBN and the formation of the CMB in providing both theoretical understanding and observational tools serves as a powerful way to test different scenarios of physics of the early universe and cosmology in general, as we will see. Especially the spectra of small inhomogeneities or temperature anisotropies of the CMB are particularly valuable.

What happened before BBN is less clear and more speculative. However, there exist good reasons to argue that the universe might have undergone an era of rapid expansion, cosmic inflation, before reaching a state which was suitable for nuclei and the CMB to form. We will discuss these aspects further in the subsequent Sections.

1.2.1 The Standard Model of particle physics

We begin by discussing the non-relativistic matter content of today's universe which can be divided into two parts: baryonic matter and non-baryonic or 'dark' matter. The known baryonic matter content is described by the Standard Model of particle physics (SM). A thorough presentation of the SM symmetries, particle content, and interactions can be found in e.g. [6, 17], and here we only review the core of the theory. Dark matter will be discussed briefly in the next Section and then more thoroughly in Chapter 2.

The gauge symmetry group of the SM is $SU_{\rm C}(3) \otimes SU_{\rm L}(2) \otimes U_{\rm Y}(1)$, where the factor $SU_C(3)$ describes the strong interactions between quarks and the corresponding gauge bosons dubbed gluons. The factor $SU_{\rm L}(2) \otimes U_{\rm Y}(1)$ describes the electroweak interaction between leptons, quarks, and the gauge bosons $Z, W^{\pm}$, and γ. The latter symmetry is spontaneously broken by the only scalar field in the theory, the Higgs field Φ, which as a result of the symmetry breaking gives mass to all SM particles except the photon γ, the neutrinos, and the gluons. Despite the fact that only quarks can construct baryons, in cosmological context the SM particles are often collectively referred to as

'baryonic matter'.

Being a quantum field theory, the SM exhibits many properties not present at classical or 'tree-level'. In particular, radiative or thermal corrections to particle masses and interactions may have major implications for particle dynamics in the early universe and for connecting dynamics at currently achievable collider energies to the very high energy scales often encountered in cosmology. These phenomena will be discussed more closely in the context where they are relevant.

The SM is not a complete theory. Most notably, it cannot accommodate dark matter [18] or generation of matter-antimatter asymmetry [19], and it is therefore expected to be an effective field theory which can be accurately used to describe particle dynamics only up to some currently unknown energy scale. Above this scale, extensions of the SM are needed to correctly describe the dynamics.

1.2.2 Other matter components

In Section 1.1 we presented the results $\Omega_{\rm m} \simeq 0.31$, $\Omega_\Lambda \simeq 0.69$ for the cosmological matter content of the universe. Observations show that the baryonic components constitute only approximately one sixth of the total non-relativistic matter content, $\Omega_{\rm b} \simeq 0.05$ [7]. Most of the non-relativistic matter content must therefore be in the form of non-baryonic and non-relativistic (cold) dark matter, whose contribution is the rest, $\Omega_{\rm CDM} \simeq 0.26$.

In today's universe only photons are relativistic[3] and contribute to radiation energy density. However, the smaller and denser the early universe was, the more particle species were relativistic and thus contributed to the energy density in the form of radiation. From cosmological observations we know that even though there is more cold dark matter than baryonic matter in today's universe, the dark matter component did not become to dominate the total energy density until $t \simeq 5 \times 10^4 y$ [7]. Thus the dynamics long before that were governed by the SM and other particles instead of the non-relativistic dark matter component.

At the moment we do not know what constitutes the cold dark matter component and how it was produced in the early universe. Overwhelming evidence for its existence and countless theoretical models and stringent experimental constraints for both its properties and origin however exist. They will be discussed in the subsequent chapters.

An even bigger mystery than dark matter is the component that constitutes the rest of the total energy density, $\Omega_\Lambda \simeq 0.69$. Currently we have no conclusive evidence for whether this component is the contribution of the vacuum energy density, dynamical dark energy, manifestation of our lack of understanding of the deeper nature of gravity, or something else[4]. Despite playing the dominant role in determining the eventual fate of today's universe – as the evolution of a depends mostly on ρ_Λ, see Eq. (1.4) –, this component played only a minor role in governing the dynamics of the early universe, and will therefore be neglected for the remainder of this thesis.

[3] Of the three neutrino generations, one may be massless and therefore constitutes radiation even today. The relativistic neutrino contribution to $\Omega_{\rm r}$ is however subdominant to photons [6, 7].

[4] An interested reader is referred to Refs. [20, 21].

1.2.3 Thermal equilibrium

In the very early universe the different SM particle species were not only relativistic but in thermal equilibrium with each other due to their relatively strong mutual interactions[5]. This equilibrium is manifested in the almost perfect blackbody distribution of the CMB, and further supported by the success of BBN calculations.

Particle species in thermal equilibrium obeyed the distribution function

$$f_i(k,T,\mu) = \frac{1}{e^{(E_i-\mu)/T} \pm 1}, \tag{1.7}$$

where $-$ and $+$ refer to bosons and fermions, respectively, and where $E_i = (k^2 + m_i^2)^{1/2}$ is the energy of particle species i, k is the corresponding momentum, and μ the chemical potential. The number and energy densities then took the form

$$n_i = \frac{g_i}{(2\pi)^3}\int f(k,T,\mu)d^3k, \qquad \rho_i = \frac{g_i}{(2\pi)^3}\int E_i(k,m_i)f(k,T,\mu)d^3k, \tag{1.8}$$

where g_i is the number of degrees of freedom of the particle species i.

By writing the effective number of degrees of freedom at temperature T as

$$g_*(T) \equiv \sum_{\text{bosons}} g_i + \frac{7}{8}\sum_{\text{fermions}} g_i, \tag{1.9}$$

the total energy density of all relativistic particles in thermal equilibrium can be written as

$$\rho = \frac{\pi^2}{30} g_* T^4. \tag{1.10}$$

These results will be used in subsequent chapters. Another result that we will use is the expression for the total entropy density

$$s = \frac{\rho + p}{T}, \tag{1.11}$$

which follows from the fundamental equation of thermodynamics. In the absence of heat transfer, the conservation of entropy in a comoving volume, $d(sa^3) = 0$, gives a useful relation between the temperature and scale factor, $T \propto g_*^{-1/3} a^{-1}$.

For successful BBN the SM has to be in thermal equilibrium and dominate the total energy density of the universe at $T \simeq 4$ MeV [22, 23] (whereas the CMB was formed at $T \simeq 0.3$ eV [7]). It may be that the SM had attained thermal equilibrium and governed the total energy density already much earlier but it is equally possible that before BBN the universe was not in thermal equilibrium at all, or that the evolution of the universe was governed by non-SM particle species, for instance particles belonging to some unknown hidden sector which later decayed to comprise the SM heat bath [24, 25]. A third option is that the SM particles attained thermal equilibrium long before BBN

[5] During BBN and the formation of the CMB, as well as during the neutrino decoupling, the universe departed from thermal equilibrium for some time. For most of the history of the early universe, however, the equilibrium was maintained.

and dominated the energy density, but there were also other matter components which were not in thermal equilibrium with the SM particles and underwent their own thermal history.

The successful BBN allows only small deviations from the known particle content. The total number of relativistic degrees of freedom at $T \simeq 1$ MeV is constrained to $N_{\rm eff} = 3.15 \pm 0.23$ [7], which is consistent with the SM value $N_{\rm eff} = 3.046$ [26]. However, there might still have been stable non-SM non-relativistic components, namely dark matter, whose abundance becomes significant only at later times. Such a scenario will be discussed in Chapters 3 and 5.

At the moment there is no conclusive evidence for how the thermal state was reached. It is, however, necessary that the universe was not in thermal equilibrium at its earliest stages but attained the thermal state only much later, as we will now discuss.

1.3 Cosmic inflation

In Section 1.1 we mentioned that the value of the sum $\sum_i \Omega_i$ is very close to unity and as a result space is essentially flat, by virtue of Eq. (1.6). At the time of BBN, $T \simeq 1$ MeV, this requires $|K| \lesssim 10^{-16}$ [6], an extremely fine-tuned initial condition.

It is therefore appealing to investigate whether there could exist a dynamical origin for this value. In fact, K is not the only parameter whose value at the time of BBN seems to require fine-tuning. The others are related to the so-called horizon (or homogeneity) and unwanted relic problems [6]. As a possible solution to these problems, one can postulate an era that preceded the period when the universe was in a thermal state: the cosmic inflation.

1.3.1 Dynamics of inflation

The main idea of cosmic inflation was first presented by the authors of [8–10]. Cosmic inflation is defined as a state of accelerated expansion of the universe, $\ddot{a} > 0$, and it is assumed to have taken place in the very early universe, typically long before BBN. By virtue of Eq. (1.6), a growing $\dot{a}$ quickly drove $K \to 0$, making the universe spatially flat. The longer the period of accelerated expansion lasted, the flatter the universe became. At the same time, the expansion made the (observable) universe nearly homogeneous and diluted the number density of unwanted relics.

As the requirement for accelerated expansion can also be expressed as $\rho + 3p < 0$ by Eq. (1.4), it has become customary to assume inflation was driven by a single scalar field with $\omega = -1$. This condition can be realized by imposing the slow-roll conditions

$$|\ddot{\phi}| \ll |H\dot{\phi}|, \qquad \dot{\phi}^2 \ll V, \tag{1.12}$$

for the scalar field ϕ, dubbed the 'inflaton', slowly rolling down its potential V. Inflation then ends when the field gains speed and the slow-roll conditions (1.12) are no longer satisfied, and the universe enters the Hot Big Bang era. This happens via a period called reheating, the process by which the SM particles attained thermal equilibrium [27, 28]. Dynamics similar to reheating will be discussed in Chapter 3.

In the literature there exist a great multitude of different inflationary models with different properties. Examples include chaotic inflation [29], hilltop inflation [30], natural inflation [31], Starobinsky inflation [32] and its variants [33, 34], and so on. Exhaustive analysis of different inflationary models can be found in e.g. [35, 36]. In this thesis we do not consider inflationary models as such but concentrate on the so-called spectator fields. Their contribution to inflationary dynamics is assumed to be negligible but they can anyway undergo dynamics whose consequences become important in the post-inflationary universe, as we will show in Chapters 3 and 5.

The duration of inflation is characterized by e-folds, $N \equiv \ln(a(t_{\rm end})/a(t))$, where $a(t_{\rm end})$ is the scale factor at the end of inflation and $a(t)$ at some earlier time t. Typical estimates for the duration of inflation vary between $N \simeq \mathcal{O}(1)...10^{16}$ [35], and usually the horizon exit of the largest observable scales is assumed to have taken place at $N \simeq 60$ [6].

At the moment we do not know how inflation began or how many inflationary periods the universe has undergone. Therefore, the main success of inflationary model resides not in solving the aforementioned fine-tuning problems, such as the flatness and homogeneity of the universe, but in explaining the origin of small temperature anisotropies present in the CMB.

1.3.2 Primordial perturbations

During inflation the inflaton field(s) acquired large quantum fluctuations. On superhorizon scales the two-point function of a single massless inflaton field froze to a constant value [6]

$$\langle \phi_{\mathbf{k}} \phi_{\mathbf{k}'} \rangle \simeq (2\pi)^3 \delta(\mathbf{k} - \mathbf{k}') \frac{H^2}{2k^3}, \tag{1.13}$$

where the subscript $\mathbf{k}$ denotes different modes of Fourier decomposition of the inflaton field ϕ. These fluctuations became classical perturbations outside the horizon and generated the perturbations which seeded the temperature anisotropies seen in the CMB [6].

The CMB perturbations can be described by considering small perturbations around the RW metric, $g_{\mu\nu} = g^{(\rm RW)}_{\mu\nu} + \delta g_{\mu\nu}$. To first order in these perturbations, the perturbed metric takes the form [37]

$$ds^2 = -(1+2A)dt^2 + 2aB_i dt dx^i + a^2\left((1-2\psi)\delta_{ij} + 2E_{ij}\right) dx^i dx^j, \tag{1.14}$$

where a is the background scale factor and the functions A, B_i, ψ, and E_{ij} describe first order perturbations around $g^{(\rm RW)}_{\mu\nu}$. The curvature perturbation in the so-called uniform density gauge can then be written as

$$\zeta \equiv -\psi - H\frac{\delta\rho}{\dot{\rho}}, \tag{1.15}$$

and it can be shown that also this quantity, in the absence of isocurvature perturbations (see the next subsection), remains constant on superhorizon scales even in the case of a massive inflaton field [6]. For Gaussian curvature perturbation ζ the statistics are fully determined by the power spectrum $\mathcal{P}_\zeta$, defined by the two-point function

$$\langle \zeta_{\mathbf{k}} \zeta_{\mathbf{k}'} \rangle \equiv (2\pi)^3 \delta(\mathbf{k}-\mathbf{k}') \frac{2\pi^2}{k^3} \mathcal{P}_\zeta(k) \simeq (2\pi)^3 \delta(\mathbf{k}-\mathbf{k}') \frac{H^2}{2k^3} \left(\frac{H}{\dot{\phi}}\right)^2, \tag{1.16}$$

where the latter equality holds for slow-roll inflation.

The results (1.13) and (1.16) allow us to write

$$\mathcal{P}_\zeta(k) = \left(\frac{H}{\dot{\phi}}\right)^2 \mathcal{P}_{\delta\phi}(k), \tag{1.17}$$

where $\mathcal{P}_{\delta\phi}(k) \equiv H_k^2/(2\pi)^2$ is the power spectrum of the inflaton field. Here H_k is the Hubble parameter at the time the scale k exited the horizon. The result (1.17) is the most important feature of the inflationary scenario, as it connects the random fluctuations of a scalar field during inflation to spatial inhomogeneities observed in the CMB, and therefore strongly supports the idea that inflation took place in the early universe.

The measured amplitude of the curvature power spectrum, $\mathcal{P}_\zeta = 2.2 \times 10^{-9}$ [38], is a stringent constraint on inflationary models. While alternative ways to generate the primordial curvature perturbation exist, such as the curvaton model [39–41] and modulated reheating scenario [42, 43], observations of the CMB are consistent with models where a single inflaton field generates the observed curvature perturbation [38].

The amplitude of the curvature power spectrum is not the only parameter which characterizes primordial dynamics. For example, the measurements of or constraints on the spectral index, $n_s(k)-1 \equiv d\mathcal{P}_\zeta/d\ln k$, the tensor-to-scalar perturbation ratio, $r \equiv \mathcal{P}_\mathcal{T}/\mathcal{P}_\zeta$, different non-gaussianity parameters, and the isocurvature power spectrum provide powerful means to describe both inflationary and post-inflationary dynamics [35, 36]. In this thesis, we concentrate on isocurvature perturbations.

1.3.3 Isocurvature perturbations

In this subsection, we follow Ref. [44] in reviewing the decomposition of a general perturbation of the matter content into adiabatic and isocurvature perturbations.

The above discussion concentrated on adiabatic perturbations, which affect all cosmological fluids such that relative ratios in the number densities between different fluid components, for example i and j, remain unperturbed, $\delta(n_i/n_j) = 0$. The adiabatic perturbation is therefore associated with the curvature perturbation via Einstein's equation (1.2), and can be shown to satisfy

$$\frac{\delta_i}{1+\omega_i} = \frac{\delta_j}{1+\omega_j}, \tag{1.18}$$

where $\delta_k \equiv \delta\rho_k/\rho_k$ is the density contrast and ω_k the corresponding equation of state parameter of the fluid component $k = i, j$. The isocurvature perturbation between the two components i and j can then be defined as departure from the adiabatic condition

$$S_{ij} = \frac{\delta_i}{1+\omega_i} - \frac{\delta_j}{1+\omega_j}, \tag{1.19}$$

when there is no heat transfer between different fluid components. We evaluate all perturbations at photon decoupling $T \simeq 0.3$ eV.

The physical content of the isocurvature perturbation can be understood as follows: because there are several cosmological fluid components, it is possible to perturb the matter content of the universe without perturbing the geometry of space. Therefore, isocurvature perturbations correspond to variations in particle number ratios, $\delta(n_i/n_j) \neq 0$, without having an effect on curvature of space.

As in the case of adiabatic perturbations, we can define a matter isocurvature power spectrum. We write it in terms of the adiabatic perturbation spectrum as

$$\mathcal{P}_S = \frac{\beta}{1-\beta}\mathcal{P}_\zeta, \tag{1.20}$$

which defines the isocurvature parameter β. For isocurvature modes uncorrelated with the adiabatic perturbations observations indicate $\beta \lesssim 0.05$ [38], which shows that the observations of the CMB are consistent with purely adiabatic perturbations. This further supports the treatment presented in Section 1.3.2.

While the non-observation of isocurvature perturbations has provided no evidence for models beyond the simplest scenario of a single-field inflation, the stringent upper bound on β provides an invaluable resource for extracting information about different particle physics scenarios describing also other than inflationary physics, as we will show in Chapters 3 and 5.

Chapter 2

Dark matter

In Section 1.2.2 we discussed the Planck observations which have revealed that there are roughly six times more non-baryonic cold dark matter, $\Omega_{\rm CDM}h^2 \simeq 0.12$, than ordinary baryonic matter, $\Omega_{\rm b}h^2 \simeq 0.02$. In this chapter, we discuss further the evidence for the existence of dark matter, different theoretical models for its production in the early universe, and the observational properties of very weakly coupled particle dark matter.

2.1 Observational evidence

In this Section we briefly review the observational evidence for dark matter following Refs. [18, 45].

The idea of dark matter as an invisible matter component dates back to the 18th century, although dynamical evidence was not to be found until the beginning of 1930's, when Kapteyn and Oort studied the motions of nearby stars and concluded that there must be an excess of gravitational pull to that the bright stars are known to cause. Ever since, an extensive number of observations of different astrophysical and cosmological targets including rotational velocities of spiral galaxies, dynamics of galaxy cluster mergers, gravitational lenses, and primordial density perturbations have all confirmed there are roughly $5-6$ times more invisible matter than visible. Evidence for dark matter is thus found to exist at all scales, both spatial and temporal. It seems therefore unlikely that, for example, models with modified laws of gravity could explain the excess of gravitational acceleration at all these different scales.

The first studies of dark matter assumed that the invisible matter content was mainly in the form of faint stars. However, evidence from the growth of primordial density fluctuations – which dark matter interferes with by modifying the so-called baryon acoustic oscillations – suggests that the observed dark matter density must consist of non-baryonic forms of matter instead of the usual baryonic matter.

What constitutes this non-baryonic matter component is, however, not known. Dark matter may or may not be composed of particles, and its properties may or may not be within the reach of current or near-future experiments. From cosmological and astrophysical observations we know that dark matter must be cold, i.e. non-relativistic, and it must have dominated the total energy density

of the universe from $T \simeq 0.8$ eV to the time when the vacuum energy density, ρ_Λ, took over. Dark matter must also be stable at cosmological scales, meaning that its lifetime must exceed $t_{\rm dec} \gtrsim 10^{26}$s. While no conclusive dark matter signals have shown up in different experiments, they have placed increasingly strong constraints on properties, such as masses and scattering cross-sections, of weakly interacting dark matter particles.

In this thesis we assume dark matter consists of one or more new quantum fields. The most studied particle dark matter candidates appearing in the literature include WIMP's (Weakly Interacting Massive Particles), sterile neutrinos, axion-like particles, moduli, and many other both theory-based and purely phenomenological models (for a recent review, see again [18]). Recently there has been substantial interest in FIMP (Feebly Interacting Massive Particle) dark matter [46, 47], which is the model we will concentrate on from Section 2.2.2 onwards.

2.2 Dark matter production

As discussed in Section 1.2.3, for most of the history of the early universe, the SM particles were in thermal equilibrium. Dark matter, on the other hand, may or may not have been part of the same heat bath. In this Section, following [4, 47], we present the two basic mechanisms for dark matter production: thermal freeze-out and non-thermal freeze-in, which are the two main cases describing scenarios where dark matter was or was not part of the SM heat bath, respectively.

To accurately solve the evolution of the dark matter relic density, one must follow the microscopic evolution of particle phase space distribution functions $f(k, t, \mu)$. The evolution is governed by Boltzmann equations, which at the level of number densities, Eq. (1.8), can be written as [4]

$$\frac{dn_i}{dt} + 3Hn_i = \frac{g}{(2\pi)^3}\int C[f]\frac{d^3k}{E}, \tag{2.1}$$

for particle species i. Here the $3Hn_i$ term accounts for the dilution of n_i due to the expansion of the universe, and the term on the right-hand side accounts for interactions that change the total number of particles. The accurate form of this so-called collision term depends on the processes relevant for the context, and will be specified later.

In general, Boltzmann equations form a coupled set of integro-differential equations for distribution functions of all particle species present, but if all but one species are assumed to be in thermal equilibrium with each other, solving the dark matter abundance reduces to a single integro-differential equation. Furthermore, once all interactions are known, solving Eq. (2.1) then gives the present-day dark matter abundance.

A minimal requirement for any dark matter model is that the solution for the contribution of particle species i yields $\Omega_i h^2 \leq 0.12$. However, there exist important cases where knowing the final abundance is not enough, but one has to solve the dark matter distribution function. In particular, this is the case for studies on the effect of dark matter on structure formation [48]. In this thesis we do not consider the dark matter yield at the particle distribution level but concentrate on solving

the resulting abundance. We will, however, comment on the consequences of some particular cases on structure formation in Section 3.2.2.

2.2.1 Freeze-out mechanism

Let us first concentrate on a widely-studied scenario: the freeze-out mechanism. In this case dark matter[1] is assumed to have initially been in thermal equilibrium with the SM particles, and the observed relic abundance is produced when the interactions between the dark matter and SM particles cannot compete with the expansion of the universe any more.

In the simplest case where dark matter undergoing thermal freeze-out consists of stable particles χ with no initial asymmetry between particles and anti-particles nor large self-interactions, the abundance can be solved simply by considering annihilation and inverse annihilation processes, $\chi\bar{\chi} \leftrightarrow \mathrm{SM}$, as they are the only processes which can change the number of χ's and $\bar{\chi}$'s in a comoving volume. For asymmetric dark matter and the effect of large self-interactions, see [49] and [50, 51], respectively.

The evolution of the dark matter number density is governed by [4]

$$\frac{dn_\chi}{dt} + 3Hn_\chi = -\langle\sigma_A|v|\rangle\left(n_\chi^2 - (n_\chi^{\mathrm{eq}})^2\right), \tag{2.2}$$

where $\langle\sigma_A|v|\rangle$ is the thermally-averaged total annihilation cross-section times velocity, n_χ is the actual dark matter number density and n_χ^{eq} is the equilibrium number density.

By defining the commonly used variables $Y \equiv n_\chi/s$ and $x \equiv m_\chi/T$ – where s is the entropy density of the bath, Eq. (1.11), and m_χ is the dark matter particle mass – Eq. (2.2) can be cast in the form

$$\frac{x}{Y_{\mathrm{eq}}}\frac{dY}{dx} = -\frac{\Gamma_A}{H}\left(\left(\frac{Y}{Y_{\mathrm{eq}}}\right)^2 - 1\right), \tag{2.3}$$

where $\Gamma_A \equiv n_\chi^{\mathrm{eq}}\langle\sigma_A|v|\rangle$ is the effective interaction rate between dark matter and bath particles.

As long as $\Gamma_A \gtrsim H$, equilibrium between the SM and dark matter particles is maintained. However, because in an expanding universe $\Gamma_A \leq H$ unavoidably occurs at some point, the annihilations will eventually shut off. We define this to take place at $x = x_f$, so that for $x \lesssim x_f$ the dark matter abundance follows the equilibrium number density, $Y \simeq Y_{\mathrm{eq}}$, while for $x \gtrsim x_f$ the dark matter abundance freezes out, $Y(x \gtrsim x_f) = Y_{\mathrm{eq}}(x_f)$. This behavior is depicted in Figure 2.1, which shows the evolution of dark matter number density for three different values of the interaction rate Γ_A.

Once dark matter falls out of thermal equilibrium, its comoving number density remains constant, $n_\chi \propto a^{-3}$. This is true for scenarios lacking the so-called dark matter cannibalization phase where number-changing interactions, such as $\chi\chi\chi \to \chi\chi$ scatterings, modify the frozen-out abundance [50]. In this Section, we neglect them for simplicity but turn back to this issue in Section 2.2.3.

[1] In fact, the use of freeze-out mechanisms is not limited to studies on dark matter production. Neutrino decoupling at $T \simeq$ MeV is an example of an early universe process where particle species underwent thermal freeze-out [4].

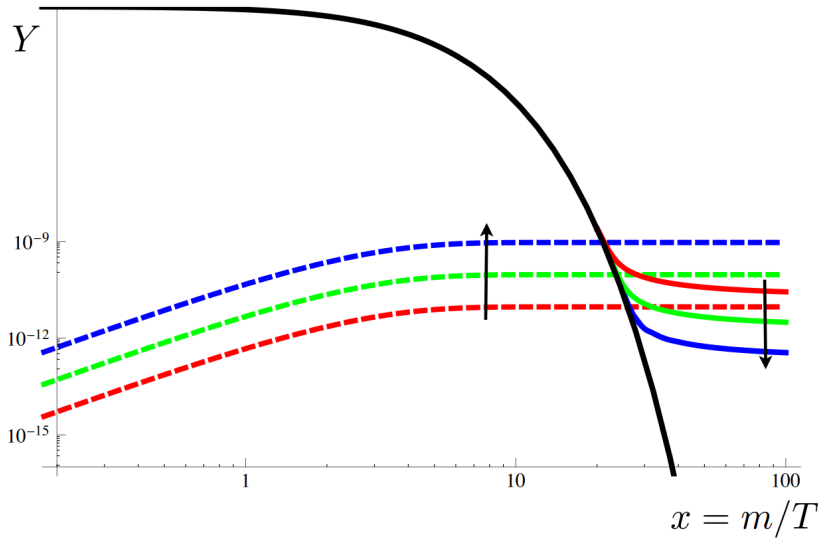

Figure 2.1: The two basic mechanisms for dark matter production: the freeze-out (solid coloured lines) and freeze-in (dashed coloured lines), for three different values of the interaction rate between the SM particles and dark matter. The arrows indicate the effect of increasing the rate for the two processes. The black solid line is the dark matter equilibrium number density. The Figure is from [47].

The standard approximate solution for the present-day abundance then becomes [4]

$$\Omega_\chi h^2 \simeq 1.07 \times 10^9 \frac{(n+1)x_f \mathrm{GeV}^{-1}}{\sqrt{g_*} M_\mathrm{P} \langle \sigma_A |v| \rangle}, \tag{2.4}$$

where $M_\mathrm{P} \equiv (8\pi G)^{-1/2}$ is the reduced Planck mass, $n = 0$ for s-wave annihilation, $n = 1$ for p-wave annihilation, and so on. Here we assumed, for simplicity, that the freeze-out occurs when dark matter is non-relativistic, $x_f \gtrsim 3$. Indeed, the dark matter freeze-out typically occurs at $x_f = 10...30$ [47].

The solution (2.4) has an important feature: the present abundance is inversely proportional to the dark matter annihilation cross-section[2]. This can be understood by remembering that in the freeze-out scenario dark matter particles are initially in thermal equilibrium with the SM particles, and the stronger the interaction between them is, the longer the dark matter particles remain in equilibrium, thus diluting their number density in an expanding universe. This can also be seen in Figure 2.1.

Maybe the most studied frozen-out dark matter candidates are supersymmetric neutralinos. Today, however, different models with frozen-out dark matter candidates (and supersymmetry in general) are beginning to be strongly constrained by experiments [18], and therefore it is not only of academic interest to start considering alternative scenarios for dark matter production.

[2]The fact that roughly a weak scale cross-section $\langle \sigma_A |v| \rangle \simeq 10^{-26} \mathrm{cm}^3 \mathrm{s}^{-1}$ yields the observed dark matter abundance is known as the 'WIMP miracle'.

2.2.2 Freeze-in mechanism

The above discussion was based on the assumption that the dark matter particles were initially in thermal equilibrium with the bath particles. However, if the coupling between the bath particles and dark matter particles is very small, interactions between them might not have been strong enough for dark matter to reach thermal equilibrium. In that case, the observed dark matter abundance has to be produced by the so-called freeze-in mechanism [1, 2, 46, 47, 52–55], instead of the freeze-out mechanism discussed above.

In the simplest case, the initial occupation number of dark matter particles is either zero or negligibly small, and the observed abundance is produced by bath particle decays[3], for instance $\sigma \to \chi\chi$ at $T \simeq m_\sigma$. Here σ is a bath particle and χ again the dark matter particle.

The freeze-in yield is active for $T \gtrsim m_\sigma/10$, and shuts off below this, as the number density of σ becomes Boltzmann-suppressed, $n_\sigma \propto \exp(-m_\sigma/T)$. By virtue of Eq. (2.1), the comoving number density of χ then becomes a constant and the dark matter abundance is said to 'freeze in'. This is again depicted in Figure 2.1.

The dark matter abundance produced by decays of bath particles, $\sigma \to \chi\chi$, is given by

$$\frac{dn_\chi}{dt} + 3Hn_\chi = \int d\Pi_\sigma d\Pi_{\chi_1} d\Pi_{\chi_2} (2\pi)^4 \delta^4(p_\sigma - p_{\chi_1} - p_{\chi_2}) |\mathcal{M}_{\sigma\to\chi\chi}|^2 \times \left(f_\sigma(1 \pm f_{\chi_1})(1 \pm f_{\chi_2}) - f_{\chi_1} f_{\chi_2}(1 \pm f_\sigma)\right), \tag{2.5}$$

where $d\Pi_i = d^3k_i/((2\pi)^3 2E_i)$ is the phase space measure for particle i, $\mathcal{M}$ is the quantum mechanical transition amplitude, and $+$ $(-)$ applies for bosons (fermions). The approximate solution for (2.5) in the limit $f_\chi \to 0$ is [47]

$$\Omega_\chi h^2 \simeq 1.09 \times 10^{27} \frac{m_\chi \Gamma_{\sigma\to\chi\chi}}{g_*^{3/2} m_\sigma^2}, \tag{2.6}$$

where all quantities are to be evaluated at $T \simeq m_\sigma$. Taking $m_\chi \ll m_\sigma$ and $\Gamma_{\sigma\to\chi\chi} = \lambda_{\sigma\chi}^2 m_\sigma/(8\pi)$, where $\lambda_{\sigma\chi}$ is the coupling strength between χ and σ, the result (2.6) yields a parametric estimate for the coupling sufficient to produce the observed dark matter abundance

$$\lambda_{\sigma\chi} \simeq 10^{-12} \left(\frac{\Omega_\chi h^2}{0.12}\right)^{1/2} \left(\frac{g_*}{10^2}\right)^{3/4} \left(\frac{m_\sigma}{m_\chi}\right)^{1/2}. \tag{2.7}$$

The implied small coupling value is compatible with the key assumption of the freeze-in scenario that the dark matter particles have not thermalized with the bath particles above $T \gtrsim m_\sigma$.

The required coupling values and assumptions of the initial abundance are not the only differences between the freeze-in and freeze-out scenarios, as also the relation between the relevant mass scale

[3] Also scattering processes, such as $AA \to \chi\chi$, where A is a bath particle, are known to contribute to the dark matter yield and dominate over particle decays if $m_\sigma < 2m_\chi$. Also mechanisms like asymmetric reheating [56] and decay of dark matter condensate [1, 2] can contribute to the dark matter yield. Here we neglect these contributions for simplicity but will include the effect of the latter process in Chapter 5.

and the bath temperature at the time of dark matter production is different. In the freeze-out mechanism the relic abundance is produced at $m_\chi/T \simeq 10 \ldots 30$, whereas for the freeze-in mechanism it arises during the epoch $m_\sigma/T \simeq 2 \ldots 5$ [47]. Also the effect for freeze-in in increasing the interaction rate between the SM and dark matter particles is contrary to the freeze-out scenario, where the larger the interaction rate was, the smaller the final abundance turned out to be. This can be clearly seen in Figure 2.1.

Moreover, because the χ particles were not in thermal equilibrium with the SM particles in the early universe, their production mechanism can be sensitive to initial conditions. This is again in contrast to the freeze-out mechanism, where thermal equilibrium destroys all dependence on the initial state of bath particles. This is an important feature of the freeze-in mechanism and we will utilize it in Chapter 5.

Also similarities arise. As with frozen-out particles, in the freeze-in scenario the frozen-in particle(s) may not be the particle(s) which comprise the final dark matter abundance: they may decay to actual dark matter particles, for example to sterile neutrinos, at a later stage [57]. The dark matter sector not being in thermal equilibrium with the SM particles may also accommodate complicated dynamics in its own sector. This would modify the final dark matter abundance, as we will now discuss.

2.2.3 Dark freeze-out

In the first studies of the freeze-in mechanism the exact value of the dark matter self-interaction coupling was considered to be irrelevant to the dark matter abundance [46, 47, 52, 53]. However, today it is known to be of utmost importance in both determining the initial conditions for low energy phenomena, as we will show in Chapter 5, and for cases where the dark matter particles interact with themselves sufficiently strongly.

If the self-interactions are large, the dark matter particles may thermalize amongst themselves and the final dark matter abundance becomes dominated not by the initial freeze-in but by a freeze-out mechanism operating within the dark matter sector; the so-called 'dark freeze-out' [3, 50, 51, 58–61]. Indeed, if the number-changing interactions, for example the $2 \to 4$ scattering processes[4], in the dark matter sector are fast, they will lead to chemical equilibrium within the dark matter sector, reducing the average momentum of the dark matter particles and increasing their number density. The dark matter abundance may therefore change even though the coupling between the SM and dark matter sectors has effectively been shut off.

It can be shown that thermalization of the hidden sector within itself will take place if the self-coupling exceeds a critical value $\lambda_{\text{crit.}} = \lambda_{\text{crit.}}(\lambda_{\sigma\chi}, m_\sigma, m_\chi)$ [3, 50, 58]. For $\lambda < \lambda_{\text{crit.}}$, the usual freeze-in picture is sufficient. If the self-coupling is larger than the critical value, the dark matter sector enters into thermal equilibrium with a hidden sector temperature T_{D}. The equilibrium is then maintained until the $4 \to 2$ interaction rate drops below the Hubble rate and the number density freezes out. The final relic abundance depends on the freeze-out temperature of the $4 \to 2$ scattering rate similarly to the standard freeze-out discussed in Section 2.2.1.

[4]Here we assume the $2 \to 3$ process is forbidden by the global $\mathbf{Z}_2$-symmetry of the dark matter field.

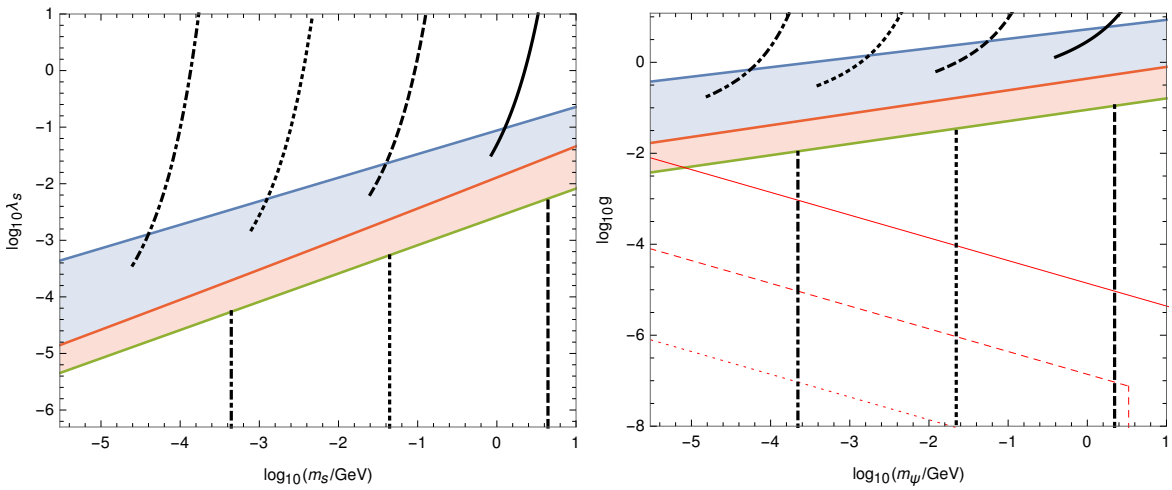

Figure 2.2: Left panel: The scalar self-coupling as a function of the scalar mass required to obtain the correct relic abundance, for different values of the coupling between the SM and dark matter sectors (the solid, dashed, dotted, and dot-dashed black lines, from smallest to largest value). In the blue shaded region the dark freeze-out happens at a relativistic temperature, $x_f < 3$; in the red shaded region the method used in [3] gives no solutions that would yield the observed dark matter abundance, and in the lower white region the dark matter abundance can be obtained via the standard freeze-in scenario. Right panel: The Yukawa coupling as a function of the fermion mass required to obtain the correct relic abundance. Below the solid, dashed and dotted red contours the dark matter sector thermalizes via scalar self-scattering before the scalars have decayed to fermions, for different values of the scalar self-interaction coupling, $\lambda_{\rm s}$, from largest to smallest. The Figure is from Ref. [3]

Depending on the matter content in the frozen-in sector, different dynamics may arise. For example, if the dark matter sector consists not only of a frozen-in scalar χ but also of a fermion ψ with a (pseudo-)scalar Yukawa coupling g to χ, either the scalar or the fermion may play the role of dark matter, depending on the hierarchy of coupling and mass values in the dark matter sector. Different scenarios are illustrated in Figures 2.2 and 2.3, where the latter further illustrates the case where dark matter is fermionic and how, in that case, the frozen-in scalars may or may not thermalize before their decay to ψ's. If they do not, then a similar bound as for the scalar self-interaction strength, $\lambda_{\rm crit.}$, can be obtained for the Yukawa coupling, $g_{\rm crit.}$ [3].

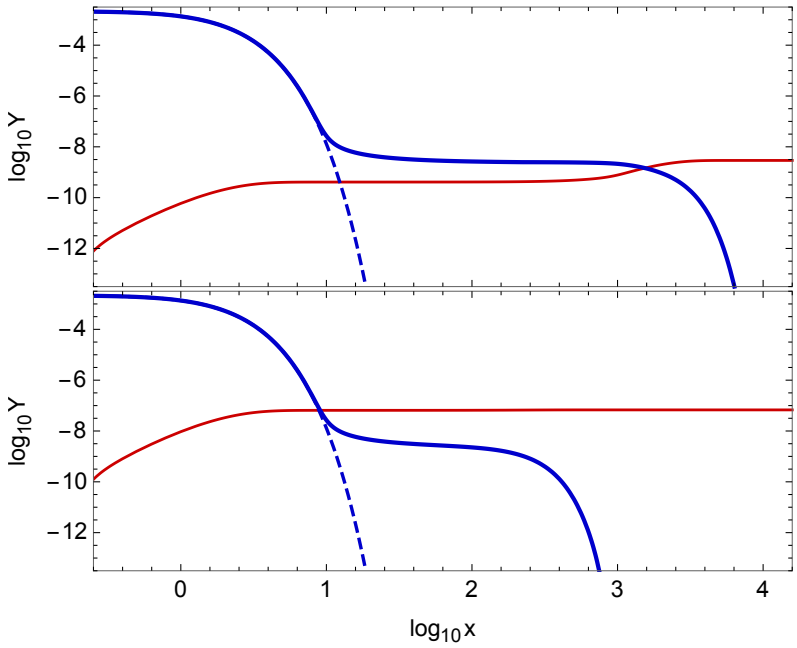

Figure 2.3: Two examples of fermionic dark matter production, requiring $m_\chi > 2m_\psi$. Upper panel: If the coupling between χ and ψ is very small, the particle production is dominated by the dark freeze-out and eventual decay of the scalar abundance (blue thick curve). In this case freeze-in operating within the hidden sector (the 'dark freeze-in') provides only a subdominant contribution to the final fermion abundance (red thin curve). Lower panel: For larger coupling values – but small enough for the fermions not to thermalize with the scalars –, the final dark matter abundance is given by the dark freeze-in. The Figure is from Ref. [3].

2.3 Observational properties of feebly coupled dark matter

For dark matter particles which interact relatively strongly with the SM particles, a large number of observational properties exist. Recoil of dark-matter particles off target nuclei; decay or annihilation signals which contribute to charged cosmic rays, photons, and neutrinos; missing energy in particle colliders; and many other phenomena have not only constraining but also discovery potential [18].

For dark matter particles which interact only very weakly with the SM particles, such as FIMP's, the observational properties are limited. However, the freeze-in mechanism also has observable consequences, even if the dark matter experiments which focus on collider signatures or direct or indirect detection would not be applicable for constraining properties of such frozen-in dark matter.

Studies on observational properties of frozen-in dark matter include the case of ultra-strongly interacting dark matter [62]; cosmological, astrophysical and collider constraints on sterile neutrinos [48, 63–66]; displaced signatures at colliders [67, 68]; and dark matter as the origin of the galactic centre gamma ray excess [69]. Frozen-in dark matter has also been used to explain the disagreement between structure formation in cold dark matter simulations and observations [70], and as an

interpretation of a spectral feature at $E \simeq 3.55$ keV observed in X-ray observations from several dark matter dominated sources [71, 72] in [73–81].

Particularly interesting is the scenario where dark matter particles have relatively strong self-interactions, as in that case astrophysical observations of galaxy cluster mergers provide an upper bound and cosmological observations of the CMB provide, in certain cases, a lower bound on dark matter self-interactions [2, 3]. Assuming that all dark matter is self-interacting, the upper bound is [82–87]

$$\frac{\sigma_{\rm DM}}{m_{\rm DM}} \lesssim 1 \frac{\rm cm^2}{\rm g}. \tag{2.8}$$

The lower bound will be discussed in Chapter 5, together with other cosmological constraints on frozen-in dark matter particles.

Furthermore, if $\sigma_{\rm DM}/m_{\rm DM}$ is close to its observational upper bound, Eq. (2.8), it might be possible to explain the shift of the gravitational centers observed for Abell 3827 [88–90] and address the so-called core-cusp [91–93], the missing satellites [94], and the too big to fail problems [95], which are classical examples of observational properties of self-interacting dark matter. Indeed, even though one would hastily conclude that a frozen-in sector would easily remain undetected, it is shown to have observational consequences. We will discuss them further in Chapter 5 in one particular scenario, in the so-called Higgs portal model, but the analysis can be easily generalized to other models of the same type.

Chapter 3

Scalar fields in the early universe

Extensions of the Standard Model of particle physics typically contain many new scalar fields on top of the only scalar field in the SM, the Higgs field. In addition to the low energy phenomenology, such as dark matter production, extended scalar sectors may have consequences for physics of the very early universe.

As discussed in Section 1.3, an obvious consequence is the cosmic inflation driven by the inflaton field(s) and the subsequent reheating process with or without modulating field(s). Even in the case where the new scalar fields do not take part in inflationary dynamics, i.e. in case the new scalars are so-called spectator fields, inflation sets non-trivial initial conditions for their post-inflationary dynamics. For example, post-inflationary phase transitions [96, 97] and dark matter production [1, 2, 98–101] are representative examples of scenarios where dynamics are sensitive to initial conditions set by inflation. In this thesis, we show how these initial conditions can be utilized to constrain SM extensions.

3.1 Quantum fields in de Sitter space

During cosmic inflation the Hubble parameter $H = \dot{a}/a$ remains constant, and as a result the universe expands exponentially, $a = \exp(Ht)$. Such a space-time is called a de Sitter space[1], and it possesses several well-known properties. In the following we will study the behavior of quantum fields, in particular the inflationary displacement of scalar fields from their vacuum state, in de Sitter space without paying much attention to fine details of several quantum effects. An exhaustive description of quantization and different quantum phenomena in de Sitter space can be found in e.g. Ref. [102].

[1] Or, in reality, a quasi-de Sitter space, as the Hubble parameter does not remain strictly constant during inflation but evolves slowly.

3.1.1 Inflationary fluctuations

We study the inflationary dynamics in a simple model described by the Lagrangian

$$\mathcal{L}_{\rm scalar} = \frac{1}{2}\partial_\mu\phi\partial^\mu\phi + \frac{1}{2}\partial_\mu\sigma\partial^\mu\sigma + \frac{\mu_\phi^2}{2}\phi^2 + \frac{\mu_\sigma^2}{2}\sigma^2 + \frac{\lambda_\phi}{4}\phi^4 + \frac{\lambda_\sigma}{4}\sigma^4 + \frac{\lambda_{\phi\sigma}}{2}\phi^2\sigma^2, \tag{3.1}$$

where both ϕ and σ are scalar fields. By assuming the inflationary scale[2] is much larger than the scalar masses, $H_* \gg \mu_\phi, \mu_\sigma$, the quadratic terms in the Lagrangian (3.1) can be neglected in investigating the scalar field dynamics during inflation. We also assume the total energy density of the scalar fields is subdominant during inflation, $V(\phi,\sigma) \ll H_*^2 M_{\rm P}^2$.

If the scalar fields are light during inflation, $d^2V/d\beta^2 \ll H_*^2$, $\beta = \phi, \sigma$, the mean fields will acquire fluctuations proportional to the inflationary scale, $\delta\beta \simeq H_*$. The dynamics can then be investigated by using the stochastic approach [103], in which one decomposes a light scalar field ϕ into super- and subhorizon parts as

$$\phi(\mathbf{x},t) = \bar{\phi}(\mathbf{x},t) + \int \frac{d^3k}{(2\pi)^3}\theta(k-aH_*)\left(\hat{a}_{\rm k}\phi_k e^{i\mathbf{k}\cdot\mathbf{x}} + \hat{a}_{\rm k}^\dagger\phi_k^* e^{-i\mathbf{k}\cdot\mathbf{x}}\right), \tag{3.2}$$

where $\hat{\phi}_k$ are the subhorizon mode functions and $\bar{\phi}$ is the field smoothed over superhorizon scales and which can therefore be regarded as a classical quantity. We assume there are no large non-minimal couplings to gravity [104] or large couplings to inflaton or other fields [105, 106], and that the Hubble rate remains constant during inflation.

The averaged field $\bar{\phi}$ then obeys the Langevin equation

$$\dot{\bar{\phi}} = -\frac{V'(\bar{\phi})}{3H_*} + f(\mathbf{x},t), \tag{3.3}$$

where the first term accounts for the classical motion and f is the stochastic noise term

$$f(\mathbf{x},t) = \frac{aH_*^2}{(2\pi)^3}\int d^3k\,\delta(k-aH_*)\left(\hat{a}_{\rm k}\phi_k e^{i\mathbf{k}\cdot\mathbf{x}} + \hat{a}_{\rm k}^\dagger\phi_k^* e^{-i\mathbf{k}\cdot\mathbf{x}}\right), \tag{3.4}$$

with the two-point correlator $\langle f(\mathbf{x},t)f(\mathbf{x},t')\rangle = H_*^3/(4\pi^2)\delta(t-t')$.

A similar treatment can be used for the inflationary behavior of the σ field. As a result, the average behavior of the fields on superhorizon scales is controlled by the Fokker-Planck equation

$$\frac{\partial P(\phi,\sigma)}{\partial t} = \sum_{\beta=\phi,\sigma}\left[\frac{H_*^3}{8\pi^2}\frac{\partial^2 P(\phi,\sigma)}{\partial\beta^2} + \frac{1}{3H_*}\frac{\partial}{\partial\beta}\left(P(\phi,\sigma)\frac{\partial V(\phi,\sigma)}{\partial\beta}\right)\right], \tag{3.5}$$

for their probability distribution $P(\phi,\sigma)$.

As the system reaches equilibrium, the distribution becomes time-independent $\partial_t P_{\rm eq.}(\phi,\sigma) = 0$, and the solution for the equilibrium distribution is given by

$$P_{\rm eq.}(\phi,\sigma) = N\exp\left(-\frac{8\pi^2 V(\phi,\sigma)}{3H_*^4}\right), \tag{3.6}$$

[2]By the inflationary scale H_*, we mean the value of the Hubble parameter at the horizon crossing of the largest observable scales, i.e. at the pivot scale $k_0 = 0.002{\rm Mpc}^{-1}$ [7].

where N is a normalization constant. For the equilibration time scale, see [107, 108].

Assuming the coupling $\lambda_{\phi\sigma}$ is small, $\lambda_{\phi\sigma} \ll \sqrt{\lambda_\phi \lambda_\sigma}$, we obtain for the root mean square values $\beta_{\rm rms} = \langle \beta^2 \rangle^{1/2}$ the result

$$\phi_{\rm rms} = \mathcal{O}(0.1) \frac{H_*}{\lambda_\phi^{1/4}} \ , \qquad \sigma_{\rm rms} = \mathcal{O}(0.1) \frac{H_*}{\lambda_\sigma^{1/4}} \ . \tag{3.7}$$

The root mean square values characterize the typical magnitudes of the scalar condensates generated during inflation. They reveal the fields are generically not in their $T = 0$ vacuum state at the end of inflation but the initial conditions for post-inflationary dynamics are given by the distribution (3.6). What exactly was, for instance, the SM Higgs field value in our local patch at the onset of post-inflationary era is not known, but we must rely on statistical analysis and assume that we do not live in an atypical universe where β_* would significantly differ from the result (3.7). This is the defining principle of our treatment in the remaining of this thesis.

3.1.2 Isocurvature limits

If the scalar fields ϕ and σ belong to two sectors which never came into thermal equilibrium with each other in the post-inflationary universe, the scalar condensate that was not in contact with the SM heat bath comprises an isocurvature mode, as discussed in Section 1.3.3. This constrains the energy density of the scalar condensate and its subsequent decay products to be very small. For clarity, let us take ϕ to be the field which comprises an isocurvature mode.

It can be shown that the Planck isocurvature bound sets a stringent bound on the particle abundance sourced by the ϕ condensate [2]

$$\frac{\Omega_{\rm i}^{(\phi_0)} h^2}{0.12} \lesssim 4.5 \times 10^{-5} \frac{\phi_*}{H_*}, \tag{3.8}$$

where ϕ_* is the primordial field value at superhorizon scales and ϕ_0 denotes the condensate. The bound (3.8) applies for $m_{\rm i} \gtrsim 1$ eV regardless of the particle species i produced by the ϕ condensate. Here we assumed that the inflationary fluctuations around the effective background field value ϕ_* have the usual spectrum of a massless scalar, $\mathcal{P}_{\delta\phi} = (H_*/2\pi)^2$, which is uncorrelated with the adiabatic perturbation spectrum, and that all other non-relativistic matter components carry adiabatic perturbation spectra.

It should be noted that the isocurvature bound (3.8) is much tighter than the dark matter overclosure limit, unless the value ϕ_* is much larger than the Hubble scale during inflation. Indeed, in Chapter 5 we will use this bound to place stringent constraints on different Higgs portal model parameters.

3.2 Post-inflationary relaxation

As shown in Section 3.1.1, scalar fields typically acquire large fluctuations during cosmic inflation and are therefore displaced from their vacuum states at the onset of the post-inflationary era. After

inflation, the fields start to relax towards their vacuum state both by getting diluted by the expansion of the universe and by decaying into particles of different kinds. Recent studies on post-inflationary evolution of such scalar condensates range from generation of the observed curvature perturbation [43, 109] or the matter-antimatter asymmetry [96, 97] to dark matter production [1, 2, 98, 99, 101], and especially the SM Higgs field relaxation towards its vacuum state has been studied extensively in the literature [110–116].

To study in more detail how and by which rate the scalars attain their vacuum values in different scenarios, we extend the model (3.1) with a fermion ψ with a pseudoscalar coupling to ϕ so that the Lagrangian becomes

$$\mathcal{L} = \mathcal{L}_{\rm scalar} + \bar{\psi}(i\partial\!\!\!/ - m_\psi)\psi + ig\phi\bar{\psi}\gamma_5\psi \ , \tag{3.9}$$

where $\mathcal{L}_{\rm scalar}$ is the scalar field Lagrangian (3.1). While the model could in principle be accommodated by any particle content and symmetry, we choose to work within this simple setup and discuss its consequences as a representative model example. The analysis can then be easily generalized to cover other interactions.

In the following we assume that the other scalar condensate, σ_0, has already decayed at the time the ϕ_0 evolution begins, and that the evolution of σ_0 does not therefore affect the decay of the ϕ_0 condensate. We also assume the inflaton field(s) decay instantaneously into SM particles at the end of inflation and reheat the universe, so that the universe becomes radiation-dominated, $\rho_{\rm tot} \propto a^{-4}$, right after inflation.

3.2.1 Field dynamics

Soon after the end of inflation the ϕ_0 condensate becomes massive, $d^2V/d\phi^2 \geq H^2$, and starts to oscillate around the minimum of its potential with an amplitude diluted by the expansion of space, as given by its equation of motion

$$\ddot{\phi}_0 + 3H\dot{\phi}_0 + \lambda_\phi\phi_0^3 + \mu_\phi^2\phi_0 = 0. \tag{3.10}$$

The scalar field sees first an effectively quartic potential $\lambda_\phi\phi_0^4 \gg \mu^2\phi_0^2$, whereas at a later stage of oscillations the quadratic mass term dominates the potential. The time of transition between these regimes is given by the condition $\lambda\phi_0^2(t_{\rm trans}) = \mu^2$. When the scalar ϕ sees an effectively quartic potential its energy density scales as radiation, $\rho_{\phi_0} \propto a^{-4}$, and when the quadratic mass term takes over the energy density scales as non-relativistic matter, $\rho_{\phi_0} \propto a^{-3}$.

The homogeneous condensate evolves in the quartic regime as

$$\phi_0(t) = \Phi_0^{(4)}(t)\mathrm{cn}(0.85\lambda_\phi^{1/2}\Phi_0(t)t, 1/\sqrt{2}), \tag{3.11}$$

where cn is the Jacobi cosine, $\Phi_0^{(4)}$ a time-dependent oscillation amplitude, and t the cosmic time, and the oscillations can be divided into multiple tones, whereas in the quadratic regime

$$\phi_0(t) = \Phi_0^{(2)}(t)\cos(\mu_\phi t), \tag{3.12}$$

and the condensate oscillates with one frequency only.

The oscillating background generates a mass term for ϕ, σ, and ψ particles

$$\begin{aligned} M_\phi^2 &= \mu_\phi^2 + 3\lambda_\phi \phi_0(t)^2, \\ M_\sigma^2 &= \mu_\sigma^2 + \frac{\lambda_{\phi\sigma}}{2}\phi_0(t)^2, \\ M_\psi^2 &= m_\psi^2 + g^2\phi_0(t)^2, \end{aligned} \tag{3.13}$$

where thermal corrections may give additional contribution to mass terms, $\mu_i = \mu_i(T)$ [117]. Here the fermionic mass term is written in a real-valued basis which requires a chiral transformation $g\phi\bar{\psi}\gamma_5\psi \to \phi\bar{\psi}(g_\mathrm{S} + ig_\mathrm{P}\gamma_5)\psi$ with $g_\mathrm{S}^2 + g_\mathrm{P}^2 = g^2$.

The additional mass terms induced by the oscillating background condensate are of particular interest, as time-dependent mass terms are known to induce particle production [118–121]. This opens up a decay channel for the homogeneous background field and may have significant consequences for post-inflationary dynamics, as we will now discuss.

3.2.2 Condensate decay and thermalization

Post-inflationary particle production from an oscillating background field has been studied to a great extent both in the context of reheating the universe after inflation and in studies related to decay of spectator fields. For example, scenarios include particle production due to parametric resonance [122–125], fermionic preheating [126–129], and geometric or tachyonic reheating [130–132]. For recent reviews, see e.g. [27, 28].

A spatially homogeneous, oscillating scalar field constitutes an effective potential for particles it couples to. To derive the corresponding perturbative decay rates, it is convenient to write the field and its square in Fourier series

$$\begin{aligned} \phi_0(t) &= \sum_{n=-\infty}^{\infty} \chi_n e^{+i\omega n t}, \\ \phi_0(t)^2 &= \sum_{n=-\infty}^{\infty} \zeta_n e^{-2i\omega n t}, \end{aligned} \tag{3.14}$$

where ω is the oscillation frequency of ϕ_0. The decay rate of the condensate energy density is given by [1, 2]

$$\Gamma_{\mathrm{s}_0} = \frac{1}{\rho_{\phi_0}} \sum_{n=1}^{\infty} \int \prod_{j=i,f} \frac{d^3p_j}{(2\pi)^3 2E_j} E_n |\mathcal{M}_n|^2 (2\pi)^4 \delta^4(p_n + \textstyle\sum_i p_i - \sum_f p_f) \prod_i f_i \prod_f (1 \pm f_f), \tag{3.15}$$

where

$$\rho_{\phi_0}(t) = \begin{cases} \frac{\lambda_\phi}{4}\Phi_0^{(4)}(t)^4, & t \gtrsim t_\mathrm{trans}\ , \\ \frac{\mu_\phi}{2}\Phi_0^{(2)}(t)^2, & t < t_\mathrm{trans}\ . \end{cases} \tag{3.16}$$

is the energy density of the condensate, $E_n = n\omega$ is the energy of the nth Fourier mode, $p_n = (E_n, 0)$, $\mathcal{M}_n$ is the amplitude[3] of the process $i \to f$ corresponding to the nth Fourier mode, f_j are phase space distribution functions, and $+$ applies for bosons and $-$ for fermions.

Specifically, the decay rates of the condensate energy density induced by the interactions $\lambda_\phi \phi_0(t)^2\phi^2$, $\lambda_{\phi\sigma}\phi_0(t)^2\sigma^2$, and $ig\phi_0(t)\bar{\psi}\gamma_5\psi$ are given by [1, 2, 121]

$$\begin{aligned}
\Gamma_{\phi_0\to\phi\phi} &= \frac{9\lambda_\phi^2\omega}{8\pi\rho_{\phi_0}}\sum_{n=1}^{\infty} n|\zeta_n|^2\sqrt{1-\left(\frac{M_\phi}{n\omega}\right)^2}, \\
\Gamma_{\phi_0\to\sigma\sigma} &= \frac{\lambda_{\phi\sigma}^2\omega}{8\pi\rho_{\phi_0}}\sum_{n=1}^{\infty} n|\zeta_n|^2\sqrt{1-\left(\frac{M_\sigma}{n\omega}\right)^2}, \\
\Gamma_{\phi_0\to\bar{\psi}\psi} &= \frac{\omega^3}{4\pi\rho_{\phi_0}}\sum_{n=1}^{\infty} n^3|\chi_n|^2\left(g_S^2\left(1-\left(\frac{2M_\psi}{n\omega}\right)^2\right)^{\frac{3}{2}} + g_P^2\sqrt{1-\left(\frac{2M_\psi}{n\omega}\right)^2}\right).
\end{aligned} \tag{3.17}$$

Finally, to account for the effect of time-dependent masses, we average all decay rates over one oscillation cycle

$$\langle\Gamma_{\phi_0\to ii}\rangle = \frac{1}{2\pi}\int_0^{2\pi/\omega}\Gamma(t)\mathrm{d}t, \tag{3.18}$$

where $i = \phi, \sigma, \psi$. Similar decay rates of the condensate energy density can be derived for particle decays induced by the condensate [1, 2], but here we neglect them for simplicity. The effect of other decay channels, such as $\phi_0 \to \phi\phi\phi$, are negligible.

The decay rates (3.17) provide not only a useful calculation method but also account for adiabatic mass terms, (3.13), in contrast to the purely perturbative decay rates studied broadly in the literature [121, 133]. The approximation, however, lacks the accurate inclusion of the backreaction of produced particles. For example, in the case of resonant, non-perturbative particle production the backreaction is known to either quickly terminate the resonant decay of the condensate [125] or lead to explosive particle production [114, 115], depending on the interaction between the condensate and other fields. The proper inclusion of particle backreaction within our semi-perturbative treatment is also expected to have a similar effect on the decay rate of the condensate energy density but a detailed study is beyond the scope of this thesis.

The evolution of the energy density of the condensate is determined by [1, 2]

$$\dot{\rho}_{\phi_0} + 3H(1+w)\rho_{\phi_0} = -\left(\langle\Gamma_{\phi_0\to\phi\phi}\rangle + \langle\Gamma_{\phi_0\to\sigma\sigma}\rangle + \langle\Gamma_{\phi_0\to\bar{\psi}\psi}\rangle\right)\rho_{\phi_0}\ , \tag{3.19}$$

where $\langle\Gamma_i\rangle$ are the decay rates of the condensate, (3.17), averaged over one oscillation. The parameter $w = 1/3$ if the condensate oscillates in the quartic regime and $w = 0$ if the condensate oscillates in the quadratic regime. In quartic regime all decay channels are open, but the $\Gamma_{\phi_0\to\bar{\psi}\psi}$ decay rate tends to be ineffective due to Pauli blocking [2]. In the quadratic regime the channel $\phi_0 \to \phi\phi$ is

[3] In the quartic regime the system is conformal and the amplitude coincides with the Minkowski result. Also in the quadratic regime we use the Minkowski metric, neglecting the small $\mathcal{O}(H/\mu_\phi)$ curvature corrections during one oscillation cycle.

always kinematically blocked. The others can be blocked as well, depending on bare mass hierarchies and possible thermal corrections in (3.13).

The solution to (3.19) is given by

$$\rho_{\phi_0} = \rho_{\phi_{\rm osc}} \left(\frac{a_{\rm osc}}{a}\right)^{3(1+w)} \exp\left(-\frac{1}{2}\int \frac{dt}{t} \sum_{i=\phi,\sigma,\psi} \frac{\langle \Gamma_{\phi_0 \to ii} \rangle (t)}{H(t)}\right), \tag{3.20}$$

where the subscript osc denotes the onset of ϕ_0 oscillations in each regime (quartic/quadratic). The decay channel for which the decay rate $\langle \Gamma_i \rangle$ becomes equal to the Hubble scale H first will therefore dominate and define the time of the condensate decay via $\langle \Gamma_i \rangle (t_{\rm dec}) = H(t_{\rm dec})$. Indeed, as seen from (3.20), the decay processes have negligible effect on the condensate evolution until $\langle \Gamma_i \rangle \simeq H$, and up to this point the background dynamics is well described by the solutions (3.11) and (3.12). When $\langle \Gamma_i \rangle \simeq H$, the amplitude of the condensate starts to decrease exponentially and to a reasonable accuracy we can model the process as an instant decay at $\langle \Gamma_i \rangle = H$.

After the condensate has decayed its decay products thermalize either with themselves or with other particle species, provided that the interactions are sufficiently strong [134, 135]. The decay products may then undergo different thermal histories depending on how they are coupled to other particles, as discussed in Section 2.2.

The above results for the dominant decay channel and time of the decay are useful not only in studying reheating dynamics or how initial conditions set by inflationary dynamics affect post-inflationary phase transitions and dark matter production but also in constraining parameters of decoupled hidden sector models, as we will discuss in Section 5. As we will show, the dependence of abundance of the produced particles on the inflationary scale constitutes a very interesting example of a scenario where new physics with a tiny coupling to the SM can be constrained by carefully investigating its dynamics both during and after inflation.

Finally, let us discuss the possibility that the scalar ϕ is very weakly coupled to the SM particles and enters the regime $\rho_{\phi_0} \propto a^{-3}$ before the matter-radiation equality at $T_{\rm eq} \simeq 0.8$ eV. In that case, its energy density may contribute to dark matter abundance in amounts which exceed the overclosure limit. This is the well-known moduli problem [136–138]. More generally, depending on the strength of the condensate's interactions, the condensate may either completely decay into particles as discussed above or survive, comprising a coherently oscillating dark matter component. The two cases could have different ramifications for structure formation [139–142], and are therefore in principle distinguishable. In the remainder of this thesis, we concentrate on a scenario where the condensate completely decays into particles.

Chapter 4

The Higgs portal model

As discussed in Section 1.2.1, the Standard Model of particle physics is not a complete theory. Most notably, it lacks an explanation for the particle nature of dark matter or for the generation of the matter–antimatter asymmetry. Therefore, the SM has to be extended, perhaps by invoking new, rather complicated symmetries. These are then assumed to exhaustively describe particle dynamics at scales higher than the range of validity of the SM, but lower than the Planck scale, where quantum gravity is expected to play an important role. Alternatively, by writing down simplified effective Lagrangians which are likely to be incomplete descriptions, one can hope to still encapsulate the most important features of the underlying theory.

In this thesis we choose the latter option. We concentrate on a hidden sector model, where new particles reside in a completely new sector which is very weakly coupled to the SM sector. If the hidden sector consists entirely of SM singlets, the possible renormalizable interactions between the SM and the hidden sector are mediated by $\Phi^\dagger\Phi$ (the Higgs portal [143–147]), $B^{\mu\nu}$ (the vector portal [147, 148]), or $\Phi^\dagger L$ (the lepton portal [147, 149]).

While all of these possibilities are equally well motivated and provide rich phenomenology both at the very high energy scales probed by cosmological observations and at lower energies currently within the reach of collider experiments, in this thesis we concentrate only on the Higgs portal model. As we will show in Chapter 5, this simple but predictive model captures many interesting features of the portal models and therefore works as a representative example of the wider class of portal scenarios.

4.1 General aspects

As discussed above, the defining property of all Higgs portal models is that the new fields couple, at tree-level, to the SM fields only via the $\Phi^\dagger\Phi$ portal. Therefore, the Higgs portal model is defined by the Lagrangian density

$$\mathcal{L} = \mathcal{L}_{\mathrm{SM}} + \mathcal{L}_{\mathrm{portal}} + f(s)\Phi^\dagger\Phi, \tag{4.1}$$

where $\mathcal{L}_{\rm SM}$ is the Lagrangian density of the visible SM sector, $\mathcal{L}_{\rm portal}$ is the Lagrangian density of the hidden portal sector which may accommodate its own symmetry groups and field content different from the SM sector, and $f(s)$ is a function which ties the SM Higgs doublet to a portal sector scalar s which we assume to be a singlet under the SM gauge interactions. In the most general renormalizable case, $f(s) = \mu_{\rm hs} s + \lambda_{\rm hs} s^2$, where $\lambda_{\rm hs}$ is a dimensionless and $\mu_{\rm hs}$ a dimensionful coupling constant determining the interaction strength between the SM Higgs doublet and the scalar s.

The hidden sector may consist of the scalar s only, or of any number of fields with their own internal symmetries. For example, there exist studies of models with s only, with sterile neutrinos, with gauge symmetries, and so on. For recent reviews, see e.g. [150, 151]. One model which we do not discuss but which is worth mentioning is the so-called mirror model [152], where the hidden sector is a replica of the visible sector with identical particle content and interactions.

While the mirror model is both predictive and testable [153], we will concentrate on a more simple class of Higgs portal models and study their phenomenology from the effective field theory point of view. Before discussing how the physics of the very early universe places stringent constraints on these kind of beyond the SM scenarios, we review the Higgs portal phenomenology studied in the literature.

4.2 Higgs portal phenomenology

The Higgs portal model is an appealing scenario because it exhibits many testable consequences. If either of the couplings $\lambda_{\rm hs}, \mu_{\rm hs}$ is large enough, some properties of the Higgs portal model can be constrained by collider, direct and indirect detection experiments. For example, the coupling $\lambda_{\rm hs} s^2 \Phi^\dagger \Phi$ allows both for the Higgs to decay invisibly into singlet scalars and for singlet scalars to annihilate into SM particles, producing fluxes of highly energetic photons originating from distant astrophysical sources. All these aspects and the constraints they impose on Higgs portal masses and coupling values have been discussed in e.g. [150, 151].

The experimental tests can be used to constrain not only the properties but also the phenomenology of the Higgs portal model; how Higgs portal fields could be responsible for various phenomena that occured in the early universe, such as dark matter production or generation of the matter–antimatter asymmetry.

4.2.1 Dark Matter

The Higgs portal scenario has been studied in the literature in the context of both the standard freeze-out and freeze-in mechanism for production of dark matter. Studies range from the singlet scalar only [46, 144, 145, 154] to a more complicated field content and phenomenology [60, 155, 156], and from ultra-cold to self-interacting dark matter [60, 157]. Because in this thesis we concentrate on the freeze-in variant, we review here only the studies on this mechanism. For a broader overview, an interested reader is again referred to Refs. [150, 151].

Earlier studies on frozen-in Higgs portal dark matter include the simple cases of the singlet scalar

only [52, 61] and a singlet fermion (sterile neutrino) [63–66, 77, 158, 159]. A frozen-in Higgs portal sector with a hidden $SU_{\rm X}(2)$ gauge symmetry was studied in Ref. [60]. In the context of Higgs portal dark matter, moduli fields (scalar condensates) were studied in Refs. [1, 2, 96].

The first studies on freeze-in production of dark matter assumed that the singlet scalar self-interaction strength is unimportant in determining the region of the parameter space of the Higgs portal model where the singlet scalar is a viable dark matter candidate. However, it was later shown to be important both in calculating the initial conditions for freeze-in production [1, 2, 96] and the final dark matter abundance [3, 60, 61], as discussed in Section 2.2.3.

In particular, dark matter self-interactions might modify the resulting abundance such that there cannot be 'FIMP miracle' – a scenario where dark matter is a self-interacting Higgs portal FIMP with a scale invariant Lagrangian [46, 55] –, as originally pointed out in [61]. However, because the proposed scenario is both elegant and economical with possible observational consequences, we plan to investigate it further in a future work.

4.2.2 Other phenomenological aspects

Other important phenomenological aspects of the Higgs portal model include the generation of the baryon asymmetry, phase transitions and the resulting production of a gravitational wave background, cosmic inflation, reheating, and generation of the observed curvature power spectrum. The list of phenomena and references we give below are not exhaustive but they are hoped to demonstrate the variety of features studied within this generic scalar extension of the SM.

In the pure SM the electroweak phase transition is known to be only a cross-over rather than a real phase transition [19, 160]. However, in the singlet scalar extension it can be made strongly first order [161, 162], and as one of the necessary conditions for any successful baryogenesis scenario is out-of-equilibrium dynamics, the Higgs portal model therefore provides for a testable platform for studies on the matter–antimatter asymmetry produced by electroweak baryogenesis [163].

The order of the electroweak phase transition is interesting not only from the baryogenesis point of view but also for the possibility of observing gravitational waves originating from a first order phase transition either in the SM sector [164] or in the hidden sector [165]. Since future space-based detectors like eLISA will have maximum sensitivity at the frequency range relevant for a first order phase transition at the electroweak scale [166], one can hope to detect gravitational waves originating not only from binary mergers [167, 168] but also from the early universe.

Other early universe phenomena studied in the Higgs portal scenario include cosmic inflation and reheating. Inflation has been studied in e.g. [34, 169–171], and even though these models typically require a sizeable non-minimal coupling to gravity, $\xi_{\rm s} s^2 R$, their inclusion is motivated also by the analysis of quantum corrections in a curved background which have been shown to generate a term of this form even if $\xi_{\rm s}$ is initially set to zero [102]. The generation of the observed curvature power spectrum by the curvaton mechanism has been studied in the Higgs portal model in e.g. [172, 173]. Hidden sector particle decays as a way to reheat the visible SM sector have recently been studied in e.g. [24, 25].

An important feature of the Higgs portal model is that while the singlet scalar can account for the observed dark matter abundance and lead to a strong first order phase transition, in light of present constraints for the dark matter abundance and from direct search experiments, these aspects cannot be realized simultaneously within the model without considerable fine-tuning [154, 174]. Cosmic inflation, on the other hand, can be realized in the singlet scalar model simultaneously with the generation of a strong first order phase transition [175] or the observed dark matter abundance [34, 170, 171].

As SM extensions with one singlet scalar only either require fine-tuning or are incapable of simultaneously explaining all the observations listed above, it is likely that substantial modifications are needed to produce a theory which could explain all phenomenology leading to the universe we observe today. As discussed above, by studying even the most minimal SM extensions one can, however, hope to still encapsulate the most important features of the underlying theory. With this in mind, we turn to derive cosmological constraints on a very weakly coupled Higgs portal model.

Chapter 5

Cosmological constraints on Higgs portal models

In order to make full use of the available constraints on new physics from collider experiments and cosmological and astrophysical observations, it is crucial to study the phenomenology of beyond the Standard Model scenarios not only at energy scales probed by current particle colliders but also at the highest energy scales that we can probe by other means, such as the scale of cosmic inflation.

Inflationary dynamics, reheating, post-inflationary phase transitions, and dark matter production are representative examples of such high energy model phenomenology, as discussed in Chapters 1, 3 and 4. Recently, the requirement of electroweak vacuum stability against inflationary fluctuations [176, 177] has also aroused significant interest in inflationary dynamics, as it provides another way to test spectator couplings. The stability conditions have been extensively studied recently in, for example, [104, 105, 111, 113, 178–186] accounting both for the non-minimal curvature coupling [104, 113, 184] as well as couplings to new physics [105, 180, 186].

In this chapter we concentrate on a Higgs portal scenario, where the hidden portal sector couples so weakly to the visible SM sector that the two sectors never became in thermal equilibrium with each other in the early universe. We study the initial conditions set by cosmic inflation and follow the relaxation of scalar condensates down to their zero-temperature vacua. This allows us to investigate what kind of model constraints arise when inflationary dynamics, dark matter production and the subsequent evolution of its abundance, as well as the requirement of stability of the scalar potential, are all combined.

5.1 The model

We assume the portal sector consists of a real singlet (pseudo-)scalar s and a fermion ψ, and that the Lagrangian is invariant under the parity transformation $\psi(t,x) \to \gamma^0\psi(t,-x)$, $s(t,x) \to -s(t,-x)$ to ensure both s and ψ can act as stable dark matter candidates. The fermionic part of the portal sector is then

$$\mathcal{L}_\psi = \bar{\psi}(i\partial\!\!\!/ - m_\psi)\psi + igs\bar{\psi}\gamma_5\psi \ , \tag{5.1}$$

and the most general renormalizable scalar potential is given by

$$V(\Phi, s) = \mu_{\rm h}^2\Phi^\dagger\Phi + \lambda_{\rm h}(\Phi^\dagger\Phi)^2 + \frac{\mu_{\rm s}^2}{2}s^2 + \frac{\lambda_{\rm s}}{4}s^4 + \frac{\lambda_{\rm hs}}{2}\Phi^\dagger\Phi s^2 \ . \tag{5.2}$$

Here Φ is again the SM Higgs doublet with the standard kinetic terms. In the unitary gauge $\sqrt{2}\Phi = (0, v+h)$, where $v = 246$ GeV at $T = 0$. We assume $\mu_{\rm s}^2 > 0$ and $m_{\rm s}^2 \equiv \mu_{\rm s}^2 + \lambda_{\rm hs}v^2/2 > 0$, so that the minimum of the potential is at $s = 0$ and $m_{\rm s}$ is the physical mass of s in the $T = 0$ vacuum. These imply an upper limit on the portal coupling, $\lambda_{\rm hs} < 2m_{\rm s}^2/v^2$. We also assume that $\lambda_{\rm h} > 0$, $\lambda_{\rm s} > 0$, and $\lambda_{\rm hs} > -2\sqrt{\lambda_{\rm h}\lambda_{\rm s}}$, guaranteeing that the tree-level potential is bounded from below. Finally, we assume $m_{\rm h} > 2m_{\rm s}$ in all cases for simplicity.

At $T < T_{\rm EW} \approx 160{\rm GeV}$ [187] the Higgs vacuum expectation value gives an additional contribution $\lambda_{\rm hs}v^2/2$ to $m_{\rm s}^2$ and $3\lambda_{\rm h}v^2$ to $m_{\rm h}^2$. At higher temperatures, interactions with the thermal bath very quickly generate a thermal mass for the Higgs condensate [188]

$$m_{\rm h}^2 = \mu_{\rm h}^2 + \frac{1}{12}\left(\frac{9}{4}g^2 + \frac{3}{4}g'^2 + 3y_{\rm t}^2 + 6\lambda_{\rm h} + \frac{1}{2}\lambda_{\rm hs}\right)T^2, \tag{5.3}$$

where T is the temperature of the SM heat bath and $g, g', y_{\rm t}$ are the SM gauge $SU(2)$, $U(1)$, and the top quark Yukawa couplings, respectively.

Because we assume the hidden sector was never in thermal equilibrium with the SM sector, requiring $|\lambda_{\rm hs}| \lesssim 10^{-7}$ [96], no similar thermal masses arise for the hidden sector particles s and ψ. In addition, the model evades current collider constraints: if $|\lambda_{\rm hs}|$ was larger, invisible decay of the Higgs boson in the LHC and the LUX experiment, measuring dark matter scattering off nuclei, would constrain the model properties [189–191], but for $|\lambda_{\rm hs}| \lesssim 10^{-7}$ this does not happen.

5.2 Initial conditions for post-inflationary dynamics

As discussed in Section 3.1, cosmic inflation sets non-trivial initial conditions for post-inflationary dynamics of scalar fields. Assuming the non-minimal curvature couplings $\xi_{\rm h}h^2R$ and $\xi_{\rm s}s^2R$ are negligible, $|\xi_{\rm h,s}| \ll 1$, we take the distribution of scalar field values at the end of inflation to be given by Eq. (3.6).

For the Higgs field this is consistent with stability of the electroweak vacuum only for $H_* \lesssim 10^{11}$ GeV, and for $H_* \gtrsim 10^{11}$ GeV stability requires $\xi_{\rm h} \gtrsim 0.1$ [104]. This renders the Higgs effectively massive and as a result no condensate is formed, $h_* = 0$ (however, see also [113]). The stability of the Higgs direction is not affected by the weakly coupled hidden sector fields and we may take $|\xi_{\rm s}| \ll 1$ irrespectively of the inflationary scale. A singlet condensate is then necessarily formed and $s_* \simeq 0.4H_*/\lambda_{\rm s}^{1/4}$ describes the typical initial field value for s after inflation, as given by Eq. (3.7).

However, the s-direction of the scalar potential may develop another minimum at a non-zero field value as the pseudo-scalar coupling g to fermions gives a negative contribution to the running of

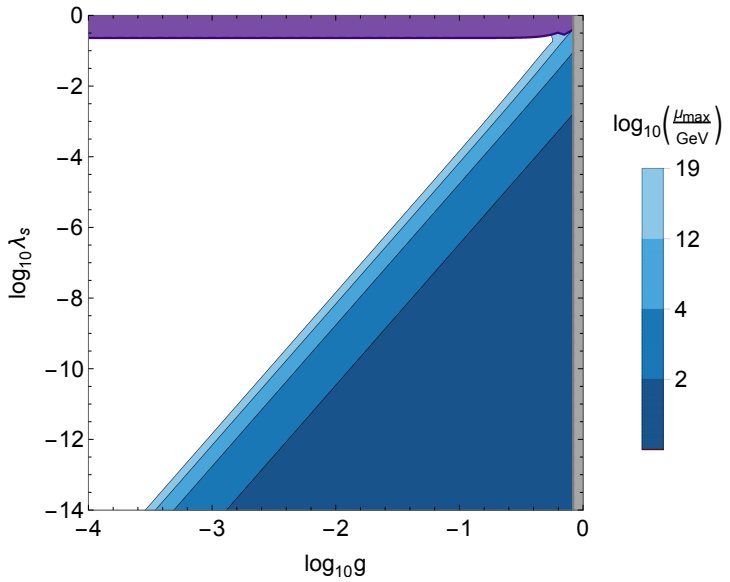

Figure 5.1: In the blue regions $\lambda_{\rm s}$ becomes negative at the scale $\mu_{\rm max}$, as indicated by the bar to the right of the plot. The axes show the values of $\lambda_{\rm s}$ and g at the scale $\mu = m_{\rm Z}$. In the purple (gray) region $\lambda_{\rm s}$ (g) has a Landau pole below the Planck scale. The Figure is from Ref. [2].

$\lambda_{\rm s}$. In the following, we restrict ourselves to the regime where the $s = 0$ vacuum is stable against inflationary fluctuations, i.e. where the scale $\mu_{\rm max}$ above which the coupling $\lambda_{\rm s}$ becomes negative is higher than the inflationary scale H_*. This imposes a constraint between g and $\lambda_{\rm s}$ as shown in Figure 5.1.

We assume again that the inflaton field(s) decay instantaneously after inflation and generate a thermal bath of SM particles. The Higgs condensate decays very rapidly at $T \simeq 0.01 T_*$ [96], and all physical processes below this temperature are insensitive to the non-vacuum initial conditions of the Higgs field. However, for s the situation is different, because it never comes into thermal equilibrium with the visible SM sector. The hidden sector may therefore accommodate dark matter which is sourced by the s_0 condensate and by non-equilibrium decays of the SM particles, and which thus is of non-thermal origin.

5.3 Higgs portal dark matter

In the scenario under consideration both the singlet scalar s and the singlet fermion ψ can be dark matter. Singlet scalar particles are generated through the decay of the primordial singlet condensate s_0, as discussed in Section 3.2.2, and through the standard freeze-in mechanism dominated by decays of Higgs particles at the electroweak scale, as discussed in Section 2.2.2. On the other hand, singlet fermions can be generated through decays of either the s_0 condensate or singlet scalar particles through the Yukawa coupling (5.1).

The dark matter abundance sourced by the primordial s_0 field is given by [2]

$$\frac{\Omega_{\rm DM}^{(\rm s0)}h^2}{0.12} \simeq 3.4\times 10^{-4} n\lambda_{\rm s}^{-1/4}\left(\frac{m_{\rm DM}}{\rm GeV}\right)\left(\frac{s_*}{10^{11}\rm GeV}\right)^{3/2}, \tag{5.4}$$

where typically $s_* \simeq 0.4H_*/\lambda_{\rm s}^{1/4}$, as given by Eq. (3.7). Here $n=1$ if the primordial field decays to s particles or if the primordial field does not decay before photon decoupling, and $n=2$ if the primordial field decays to fermions directly or via the process $s_0 \to 2s \to 4\psi$. Whether the primordial field decays to scalars or fermions depends on the coupling strengths. It should be noted that for reasonable parameter values, $\lambda_{\rm s}, g \gtrsim 10^{-8}$, the s_0 condensate typically decays at temperatures above the electroweak scale.

The standard freeze-in production at the electroweak scale is dominated by decays of Higgs particles. In this case the dark matter abundance produced by the freeze-in mechanism is [58]

$$n_{\rm D}^{\rm initial} \simeq 3\frac{n_{\rm h}^{\rm eq}\Gamma_{h\to ss}}{H}\bigg|_{T=m_{\rm h}}, \tag{5.5}$$

where $n_{\rm h}^{\rm eq}$ is the Higgs equilibrium number density and the expression is evaluated when the temperature of the SM heat bath is $T \approx m_{\rm h}$. Here the Higgs decay width into s particles is given by the standard expression $\Gamma_{h\to ss} = \lambda_{\rm hs}^2 v^2/32\pi m_{\rm h}$ at the limit $m_{\rm s} \ll m_{\rm h}$.

In the limit of small self-interactions, $\lambda_{\rm s}, g \ll 1$, the dark matter abundance sourced by Higgs decays then becomes

$$\frac{\Omega_{\rm DM}^{(\rm fi)}h^2}{0.12} = 5.3\times 10^{21} n\lambda_{\rm hs}^2\left(\frac{m_{\rm DM}}{\rm GeV}\right), \tag{5.6}$$

in accord with Eq. (2.6). Here again $n=1$ for scalars and $n=2$ for fermions. In this limit, one can simply sum the yields from the scalar condensate, (5.4), and Higgs decay, (5.6) to obtain

$$\Omega_{\rm DM} = \Omega_{\rm DM}^{(\rm s0)} + \Omega_{\rm DM}^{(\rm fi)}. \tag{5.7}$$

In the standard freeze-in scenario the summation (5.7) indeed gives the final relic abundance that diluted only with the scale factor after the production of dark matter through the s_0 condensate and Higgs particle decays had stopped. However, if the number changing interactions – i.e. the $2 \leftrightarrow 4$ scattering processes in the hidden sector – are fast, they will lead to a chemical equilibrium within the hidden sector, reducing the average momentum of the dark matter particles and increasing their number density, as described in Section 2.2.3. Eventually, this will lead to dark freeze-out, where the final dark matter abundance becomes determined by the freeze-out mechanism operating within the hidden sector.

The dark freeze-out temperature, $x_{\rm D}^{\rm FO} \equiv m_{\rm DM}/T_{\rm D}^{\rm FO}$ can be solved by invoking the fact that after the Higgs decays have stopped and the hidden sector has reached equilibrium within itself the entropies of both sectors are conserved separately, and hence the ratio of the entropy densities $\chi \equiv s/s_{\rm D}$ remains constant. This can be cast as an equation for the dark freeze-out temperature in terms of the dark matter abundance [50]

$$x_{\mathrm{D}}^{\mathrm{FO}} = \frac{m_{\mathrm{s}}}{3.6\ \mathrm{eV}\ \Omega_{\mathrm{DM}} h^2 \chi}, \tag{5.8}$$

where, by energy conservation, χ can be expressed in terms of the initial value of $\xi \equiv T_{\mathrm{D}}/T = (g_* \rho_{\mathrm{D}}/(\rho g_{*\mathrm{D}}))^{1/4}$ at $T = m_{\mathrm{h}}/3$.

On the other hand, the dark freeze-out temperature can be estimated as the temperature at which the $4 \to 2$ interaction rate drops below the Hubble rate, resulting in [3]

$$x_{\mathrm{D}}^{\mathrm{FO}} = \frac{1}{3} \log \left(\left(\frac{1}{2\pi} \right)^{\frac{9}{2}} \frac{C \xi^2 M_{\mathrm{P}}}{1.66 \sqrt{g_*} (x_{\mathrm{D}}^{\mathrm{FO}})^{\frac{5}{2}}} \right), \tag{5.9}$$

where $C = \lambda_{\mathrm{s}}^4 / m_{\mathrm{s}}$ for scalars and $C = g^8 m_\psi^9 / m_{\mathrm{s}}^{10}$ for fermions. Here we assumed that in the fermionic case the scalar self-scatterings are irrelevant for thermalization of the hidden sector.

Equating (5.8) with (5.9) and requiring the dark matter abundance match observations, $\Omega_{\mathrm{DM}} h^2 = 0.12$, yields a relation between the three parameters of the model, $m_{\mathrm{s}}, \lambda_{\mathrm{s}}, \lambda_{\mathrm{hs}}$, if dark matter consists of scalar particles, or between the five parameters $m_\psi, m_{\mathrm{s}}, g, \lambda_{\mathrm{s}}, \lambda_{\mathrm{hs}}$, if dark matter consists of fermions. This relation is an important feature of the dark freeze-out mechanism, as it provides a powerful mean to extract information about sectors whose constituents are very weakly coupled to the SM particles and whose properties would therefore be very hard to constrain by current collider experiments.

This relation is not only of theoretical interest but can be connected to observations. As discussed in Section 3.1.2, if the scalar s belongs to a sector which never reached thermal equilibrium with the SM heat bath, it comprises an isocurvature mode. Dark matter production from the singlet condensate is therefore strictly constrained by the limit (3.8), but the singlet particles can still constitute all dark matter when most of the abundance is sourced by the standard freeze-in mechanism and only a small fraction by decay of the primordial scalar field. This notion provides a unique way to place both cosmological and astrophysical constraints on weakly coupled Higgs portal scenarios.

5.4 Cosmological and astrophysical constraints

In this last Section, we show how stringent constraints for hidden sector properties can be derived even if the sector interacts very weakly with the SM particles.

By connecting the result (5.4) for dark matter abundance produced by decay of a primordial scalar condensate to the isocurvature limit (3.8) and requiring that we do not live in an atypical universe[1], we obtain

$$\lambda_{\mathrm{s}} \gtrsim \left(\frac{n}{6} \right)^{8/3} \left(\frac{m_{\mathrm{DM}}}{\mathrm{GeV}} \right)^{8/3} \left(\frac{H_*}{10^{11} \mathrm{GeV}} \right)^4, \tag{5.10}$$

i.e. cosmological constraints imply a lower bound on the scalar self-interaction strength. If the value of λ_{s} were smaller than this limit, the CMB would exhibit an excess of isocurvature modes.

[1] See Ref. [3] for a quantitative definition of 'atypical'.

The result (5.10) applies for both scalar and fermion dark matter in the Higgs portal model under consideration. For similar isocurvature constraints, see [192, 193].

On the other hand, as discussed in Section 2.3, astrophysical observations provide an upper bound on dark matter self-interactions, $\sigma_{\rm DM}/m_{\rm DM} \lesssim 1{\rm cm}^2/{\rm g}$. In the limit $m_{\rm s} \ll m_{\rm h}$, $g^2 m_\psi/m_{\rm s} \ll 1$ the scalar and fermion self-interaction cross-sections divided by the corresponding masses are

$$\frac{\sigma_{\rm s}}{m_{\rm s}} \simeq \frac{9\lambda_{\rm s}^2}{32\pi m_{\rm s}^3}, \qquad\qquad \frac{\sigma_\psi}{m_\psi} \simeq \frac{g^4 m_\psi}{4\pi m_{\rm s}^4}, \tag{5.11}$$

so that together the cosmological and astrophysical constraints imply

$$4\times 10^{-8}\left(\frac{m_{\rm s}}{10{\rm MeV}}\right)^{8/3}\left(\frac{H_*}{10^{11}{\rm GeV}}\right)^4 \lesssim \lambda_{\rm s} \lesssim 0.2\left(\frac{m_{\rm s}}{10{\rm MeV}}\right)^{3/2}, \tag{5.12}$$

if the scalar s comprises the observed dark matter abundance and

$$\frac{m_\psi}{\rm GeV} \lesssim \begin{cases} 5.9\times 10^4 g^{-4}(m_{\rm s}/{\rm GeV})^4, \\ 3\lambda_{\rm s}^{3/8}(H_*/10^{11}{\rm GeV})^{-3/2}, \end{cases} \tag{5.13}$$

if the fermion ψ constitutes the dark matter relic density. Here the first limit on the fermion mass is given by the dark matter self-interaction limit (2.8) and the second by the isocurvature bound (5.10). A lower bound arises from Lyman-α forest data, which excludes warm dark matter with mass below $m_{\rm DM} \approx 3$ keV [194]. For fermions, no lower bound on g can be imposed.

The lower bound on $\lambda_{\rm s}$, (5.10), implies that we can expect scalar dark matter to have sufficiently large self-interactions. This has immediate consequences both for the process that determines the generation of the observed dark matter abundance, and, on the observational side, on structure formation, as discussed in Section 2.3. The imposed bounds on parameter space are depicted in Figure 5.2 together with the relic abundance in different cases. The region to the right of the gray contours is ruled out by the non-observation of isocurvature perturbations.

The isocurvature constraint (3.8) applies as such if the comoving number densities of the singlet particles produced by the decay of the primordial condensate and via the freeze-in mechanism are separately conserved. If the hidden sector thermalizes within itself, bounds similar to (5.12) and (5.13) can be derived by comparing the energy density carried by the particles produced from the primordial condensate to the energy density of the particles produced via the freeze-in mechanism, at the time of the hidden sector thermalization [3]. The effect of this correction is to increase the importance of the isocurvature constraint. Because thermalization of the hidden sector results in a larger final abundance than in the standard freeze-in scenario, in order to produce the observed dark matter abundance a smaller initial abundance of particles is needed. Thus, for given $\lambda_{\rm hs}$, an initial abundance produced from the decay of the primordial condensate will contribute a larger fraction of the total dark matter relic density than it would in the standard freeze-in scenario. This is seen in the shift of the gray contours above the red shaded region in Figure 5.2.

We emphasize that the formation of primordial condensates is a typical consequence in a theory which contains scalar fields. Therefore, it is expected that qualitatively similar results constrain the

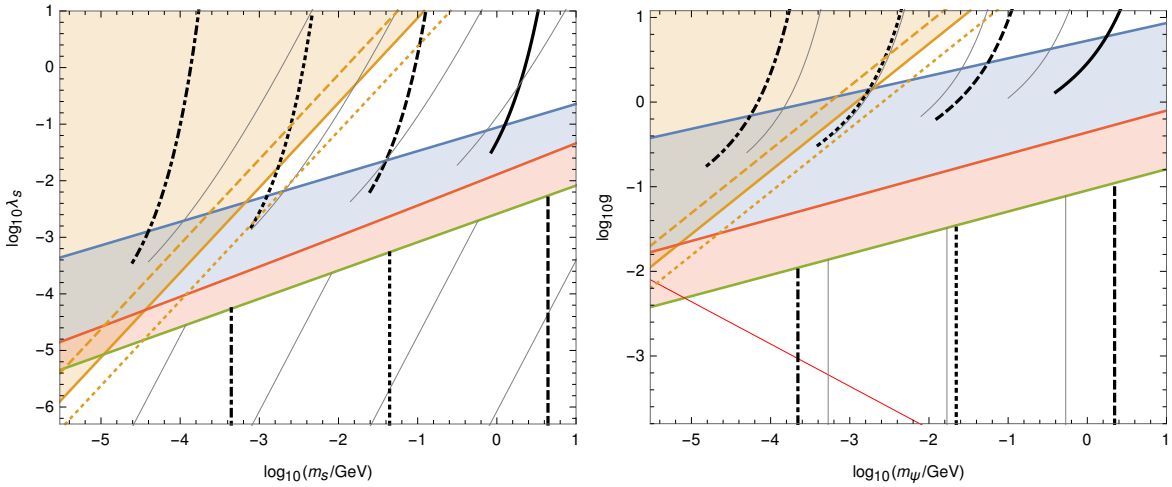

Figure 5.2: Left panel: The self-interaction bound and isocurvature constraints for the scalar dark matter scenario. The self-interaction limit, $\sigma_{\rm DM}/m_{\rm DM} < 1$ cm^2/g, is shown by the yellow shaded region in the top left corner together with the $\sigma_{\rm DM}/m_{\rm DM} = 10, 0.1$ cm^2/g contours (dashed and dotted, respectively), and the isocurvature constraints by the gray contours for $H_* = 10^{13}, 10^{12}, 10^{11}, 10^{10}$ GeV from left to right. The blue and red regions correspond to those in Figure 2.2. The black contours show $\lambda_{\rm hs} = 10^{-9}, 10^{-10}, 10^{-11}, 10^{-12}$ from left to right. Right panel: Same as the left panel for the case of fermion dark matter. The red contour marks the thermalization via scalar self-scattering for $\lambda_{\rm s} = 0.1$. In this figure $m_{\rm s} = 10 m_\psi$, and $\lambda_{\rm s} = 0.01$ for the isocurvature contours. The Figure is from Ref. [3].

masses and couplings also in other, more generic portal type extensions of the SM.

As we have discussed, constraints of such cosmological origin arise by virtue of the non-thermalization of the hidden sector with the visible SM one. If the two sectors thermalize, all information about initial conditions is lost and as a result no such constraints can be derived[2]. Even in that case, the hope in investigating the properties of beyond the SM physics does not lie only in the future success of different collider and direct and indirect detection experiments, but also in other cosmological observables related not only to dark matter but also to cosmic inflation, gravitational waves originating from early universe phase transitions [164, 165], and, for instance, the large scale structure of the universe [195, 196]. The above results apply as such to weakly coupled dark matter models only, but they show how information about particle physics models can be extracted from cosmological observables even in the case where the connection between new physics and the known SM sector is not within the reach of the current or near-future direct experiments.

[2]In this sense, the cosmological constraints arise not even with but *because* of their tiny coupling to the visible SM sector.

Chapter 6

Conclusions and outlook

In this thesis we have considered the observational consequences of a Higgs portal scenario where the new physics interacts very weakly with the particle content of the Standard Model of particle physics. In particular, we concentrated on the observational properties of self-interacting, initially non-thermal Higgs portal dark matter. We showed that many of the cosmologically interesting features of portal scenarios are captured already by the simplest effective model featuring a singlet scalar s coupled to the SM Higgs via $\lambda s^2 \Phi^\dagger \Phi$. We also extended the model to cover fermionic dark matter.

These simple extensions of the SM have been proven to have interesting phenomenological and observational consequences. The new dark matter candidates may originate not only from decays or annihilations of the SM bath particles, but also from non-thermal production of particles from a primordial scalar condensate formed during cosmic inflation. Additionally, the non-zero self-interactions may lead to thermalization within the hidden sector, resulting in a scenario where the observed dark matter abundance is determined by a freeze-out mechanism operating within the hidden sector, the 'dark freeze-out', instead of the standard freeze-in or freeze-out scenarios.

Because typically part of the relic abundance originates from non-thermal particle production from a primordial scalar condensate, we were able to derive a novel connection between the scale of inflation and the dark matter abundance, Eq. (5.4), and use it to place stringent constraints on viable mass scales and coupling values in SM extensions with a very weakly coupled hidden sector. Because such a primordial condensate generically comprises an isocurvature mode whose contribution to the observed dark matter abundance is strictly constrained by observations of the Cosmic Microwave Background, the derived constraints are much stronger than the dark matter overclosure bound. The bounds (5.12) and (5.13), together with the numerical results depicted in Figure 5.2, which combine the isocurvature limits with astrophysical constraints can therefore be considered to be our main results.

The dependence of Higgs portal dark matter on the inflationary dynamics therefore constitutes an example of a SM extension where new physics even with a tiny coupling to the SM can be constrained by carefully investigating its dynamics both during and after inflation. We emphasize that the derived bounds are generic to most weakly coupled portal models with light scalar fields, and that qualitatively similar results are expected to arise also in other portal extensions of the SM.

The freeze-in mechanism we concentrated on is clearly falsifiable. It is, however, of key importance to look for properties of different models which could also verify the scenario – if not by collider experiments, by cosmological and astrophysical observations. Work remains to be done also in further investigating frozen-in hidden sectors with even more structure, such as broken or unbroken gauge interactions and different mass hierarchies.

The ongoing and planned CMB polarization experiments will probe the amplitude of primordial tensor perturbations down to $r \lesssim 10^{-3}$ [197, 198], corresponding to an inflationary scale $H_* \sim 10^{13}$ GeV. As we have shown, a positive observation would affect not only models of inflation, but also generic SM extensions which include light scalar fields that are very weakly coupled to the SM sector. In addition, the forthcoming European Space Agency's satellite Euclid, with a launch date in 2020, will provide new cosmological data in large amounts [199]. It will map the large scale structure and the dark matter content of the universe, and is therefore expected to yield valuable new information about dark energy and dark matter, and thus about the universe as a whole.

A careful investigation of the observational consequences of weakly coupled hidden sector models could suggest powerful new tests of specific SM extensions. With the aid of the near-future missions mentioned above, they might provide understanding of new physics at scales which exceed the current particle collider energies by several magnitudes. This could play important role in connecting particle physics to cosmology: linking the microscopic evolution at the smallest length scales to the evolution of the cosmos itself.

Bibliography

[1] Sami Nurmi, Tommi Tenkanen, and Kimmo Tuominen. Inflationary Imprints on Dark Matter. *JCAP*, 1511(11):001, 2015, 1506.04048.

[2] Kimmo Kainulainen, Sami Nurmi, Tommi Tenkanen, Kimmo Tuominen, and Ville Vaskonen. Isocurvature Constraints on Portal Couplings. *JCAP*, 1606(06):022, 2016, 1601.07733.

[3] Matti Heikinheimo, Tommi Tenkanen, Kimmo Tuominen, and Ville Vaskonen. Observational Constraints on Decoupled Hidden Sectors. *Phys. Rev.*, D94:063506, 2016, 1604.02401.

[4] Edward W. Kolb and Michael S. Turner. *The Early Universe*. Addison-Wesley, 1990.

[5] Sean M. Carroll. *Spacetime and geometry: An introduction to general relativity*. Addison-Wesley, 2004.

[6] David H. Lyth and Andrew R. Liddle. *The primordial density perturbation: Cosmology, inflation and the origin of structure*. Cambridge University Press, 2009.

[7] P. A. R. Ade et al. Planck 2015 results. XIII. Cosmological parameters. *Astron. Astrophys.*, 594:A13, 2016, 1502.01589.

[8] Alexei A. Starobinsky. Spectrum of relict gravitational radiation and the early state of the universe. *JETP Lett.*, 30:682–685, 1979. [Pisma Zh. Eksp. Teor. Fiz.30,719(1979)].

[9] Alan H. Guth. The Inflationary Universe: A Possible Solution to the Horizon and Flatness Problems. *Phys. Rev.*, D23:347–356, 1981.

[10] Andrei D. Linde. A New Inflationary Universe Scenario: A Possible Solution of the Horizon, Flatness, Homogeneity, Isotropy and Primordial Monopole Problems. *Phys. Lett.*, B108:389–393, 1982.

[11] V. Springel, S. D. M. White, A. Jenkins, C. S. Frenk, N. Yoshida, L. Gao, J. Navarro, R. Thacker, D. Croton, J. Helly, J. A. Peacock, S. Cole, P. Thomas, H. Couchman, A. Evrard, J. Colberg, and F. Pearce. Simulations of the formation, evolution and clustering of galaxies and quasars. *Nature*, 435:629–636, 2005, astro-ph/0504097.

[12] Gary Steigman. Primordial Nucleosynthesis in the Precision Cosmology Era. *Ann. Rev. Nucl. Part. Sci.*, 57:463–491, 2007, 0712.1100.

[13] Adam G. Riess et al. A 2.4% Determination of the Local Value of the Hubble Constant. *Astrophys. J.*, 826(1):56, 2016, 1604.01424.

[14] Jose Luis Bernal, Licia Verde, and Adam G. Riess. The trouble with H_0. *JCAP*, 1610(10):019, 2016, 1607.05617.

[15] Vladimir V. Luković, Rocco D'Agostino, and Nicola Vittorio. Is there a concordance value for H_0? *Astron. Astrophys.*, 595:A109, 2016, 1607.05677.

[16] Thomas Tram, Robert Vallance, and Vincent Vennin. Inflation Model Selection meets Dark Radiation. 2016, 1606.09199.

[17] Michael W. Peskin and Daniel V. Schroeder. *An Introduction to Quantum Field Theory*. Westview Press, 1995.

[18] Michael Klasen, Martin Pohl, and Günter Sigl. Indirect and direct search for dark matter. *Prog. Part. Nucl. Phys.*, 85:1–32, 2015, 1507.03800.

[19] K. Kajantie, M. Laine, K. Rummukainen, and Mikhail E. Shaposhnikov. Is there a hot electroweak phase transition at m(H) larger or equal to m(W)? *Phys.Rev.Lett.*, 77:2887–2890, 1996, hep-ph/9605288.

[20] Martin Kunz. The phenomenological approach to modeling the dark energy. *Comptes Rendus Physique*, 13:539–565, 2012, 1204.5482.

[21] Yue-Yao Xu and Xin Zhang. Comparison of dark energy models after Planck 2015. *Eur. Phys. J.*, C76:588, 2016, 1607.06262.

[22] M. Kawasaki, Kazunori Kohri, and Naoshi Sugiyama. MeV scale reheating temperature and thermalization of neutrino background. *Phys. Rev.*, D62:023506, 2000, astro-ph/0002127.

[23] Steen Hannestad. What is the lowest possible reheating temperature? *Phys. Rev.*, D70:043506, 2004, astro-ph/0403291.

[24] Asher Berlin, Dan Hooper, and Gordan Krnjaic. PeV-Scale Dark Matter as a Thermal Relic of a Decoupled Sector. *Phys. Lett.*, B760:106–111, 2016, 1602.08490.

[25] Tommi Tenkanen and Ville Vaskonen. Reheating the Standard Model from a hidden sector. *Phys. Rev.*, D94(8):083516, 2016, 1606.00192.

[26] Gianpiero Mangano, Gennaro Miele, Sergio Pastor, Teguayco Pinto, Ofelia Pisanti, and Pasquale D. Serpico. Relic neutrino decoupling including flavor oscillations. *Nucl. Phys.*, B729:221–234, 2005, hep-ph/0506164.

[27] Rouzbeh Allahverdi, Robert Brandenberger, Francis-Yan Cyr-Racine, and Anupam Mazumdar. Reheating in Inflationary Cosmology: Theory and Applications. *Ann. Rev. Nucl. Part. Sci.*, 60:27–51, 2010, 1001.2600.

[28] Mustafa A. Amin, Mark P. Hertzberg, David I. Kaiser, and Johanna Karouby. Nonperturbative Dynamics Of Reheating After Inflation: A Review. *Int. J. Mod. Phys.*, D24:1530003, 2014, 1410.3808.

[29] Andrei D. Linde. Chaotic Inflation. *Phys. Lett.*, B129:177–181, 1983.

[30] Lotfi Boubekeur and David.H. Lyth. Hilltop inflation. *JCAP*, 0507:010, 2005, hep-ph/0502047.

[31] Katherine Freese, Joshua A. Frieman, and Angela V. Olinto. Natural inflation with pseudo - Nambu-Goldstone bosons. *Phys. Rev. Lett.*, 65:3233–3236, 1990.

[32] Alexei A. Starobinsky. A New Type of Isotropic Cosmological Models Without Singularity. *Phys. Lett.*, B91:99–102, 1980.

[33] Fedor L. Bezrukov and Mikhail Shaposhnikov. The Standard Model Higgs boson as the inflaton. *Phys. Lett.*, B659:703–706, 2008, 0710.3755.

[34] Rose Natalie Lerner and John McDonald. Gauge singlet scalar as inflaton and thermal relic dark matter. *Phys. Rev.*, D80:123507, 2009, 0909.0520.

[35] Anupam Mazumdar and Jonathan Rocher. Particle physics models of inflation and curvaton scenarios. *Phys. Rept.*, 497:85–215, 2011, 1001.0993.

[36] Jerome Martin, Christophe Ringeval, and Vincent Vennin. Encyclopaedia Inflationaris. *Phys. Dark Univ.*, 5-6:75–235, 2014, 1303.3787.

[37] Viatcheslav F. Mukhanov, H. A. Feldman, and Robert H. Brandenberger. Theory of cosmological perturbations. Part 1. Classical perturbations. Part 2. Quantum theory of perturbations. Part 3. Extensions. *Phys. Rept.*, 215:203–333, 1992.

[38] P. A. R. Ade et al. Planck 2015 results. XX. Constraints on inflation. *Astron. Astrophys.*, 594:A20, 2016, 1502.02114.

[39] Kari Enqvist and Martin S. Sloth. Adiabatic CMB perturbations in pre - big bang string cosmology. *Nucl. Phys.*, B626:395–409, 2002, hep-ph/0109214.

[40] David H. Lyth and David Wands. Generating the curvature perturbation without an inflaton. *Phys. Lett.*, B524:5–14, 2002, hep-ph/0110002.

[41] Takeo Moroi and Tomo Takahashi. Effects of cosmological moduli fields on cosmic microwave background. *Phys. Lett.*, B522:215–221, 2001, hep-ph/0110096. [Erratum: Phys. Lett.B539,303(2002)].

[42] Gia Dvali, Andrei Gruzinov, and Matias Zaldarriaga. A new mechanism for generating density perturbations from inflation. *Phys. Rev.*, D69:023505, 2004, astro-ph/0303591.

[43] Andrea De Simone and Antonio Riotto. Cosmological Perturbations from the Standard Model Higgs. *JCAP*, 1302:014, 2013, 1208.1344.

[44] D. Langlois. Isocurvature cosmological perturbations and the CMB. *Comptes Rendus Physique*, 4:953–959, 2003.

[45] Gianfranco Bertone and Dan Hooper. A History of Dark Matter. 2016, 1605.04909.

[46] John McDonald. Thermally generated gauge singlet scalars as selfinteracting dark matter. *Phys.Rev.Lett.*, 88:091304, 2002, hep-ph/0106249.

[47] Lawrence J. Hall, Karsten Jedamzik, John March-Russell, and Stephen M. West. Freeze-In Production of FIMP Dark Matter. *JHEP*, 1003:080, 2010, 0911.1120.

[48] Alexander Merle and Maximilian Totzauer. keV Sterile Neutrino Dark Matter from Singlet Scalar Decays: Basic Concepts and Subtle Features. *JCAP*, 1506:011, 2015, 1502.01011.

[49] Kathryn M. Zurek. Asymmetric Dark Matter: Theories, Signatures, and Constraints. *Phys. Rept.*, 537:91–121, 2014, 1308.0338.

[50] Eric D. Carlson, Marie E. Machacek, and Lawrence J. Hall. Self-interacting dark matter. *Astrophys. J.*, 398:43–52, 1992.

[51] Duccio Pappadopulo, Joshua T. Ruderman, and Gabriele Trevisan. Dark matter freeze-out in a nonrelativistic sector. *Phys. Rev.*, D94(3):035005, 2016, 1602.04219.

[52] Carlos E. Yaguna. The Singlet Scalar as FIMP Dark Matter. *JHEP*, 1108:060, 2011, 1105.1654.

[53] Mattias Blennow, Enrique Fernandez-Martinez, and Bryan Zaldivar. Freeze-in through portals. *JCAP*, 1401:003, 2014, 1309.7348.

[54] Fatemeh Elahi, Christopher Kolda, and James Unwin. UltraViolet Freeze-in. *JHEP*, 03:048, 2015, 1410.6157.

[55] Zhaofeng Kang. View FImP miracle (by scale invariance) a la self-interaction. *Phys. Lett.*, B751:201–204, 2015, 1505.06554.

[56] Peter Adshead, Yanou Cui, and Jessie Shelton. Chilly Dark Sectors and Asymmetric Reheating. *JHEP*, 06:016, 2016, 1604.02458.

[57] R. Adhikari et al. A White Paper on keV Sterile Neutrino Dark Matter. *Submitted to: White paper*, 2016, 1602.04816.

[58] Xiaoyong Chu, Thomas Hambye, and Michel H. G. Tytgat. The Four Basic Ways of Creating Dark Matter Through a Portal. *JCAP*, 1205:034, 2012, 1112.0493.

[59] Yonit Hochberg, Eric Kuflik, Tomer Volansky, and Jay G. Wacker. Mechanism for Thermal Relic Dark Matter of Strongly Interacting Massive Particles. *Phys. Rev. Lett.*, 113:171301, 2014, 1402.5143.

[60] Nicolas Bernal, Xiaoyong Chu, Camilo Garcia-Cely, Thomas Hambye, and Bryan Zaldivar. Production Regimes for Self-Interacting Dark Matter. *JCAP*, 1603(03):018, 2016, 1510.08063.

[61] Nicolas Bernal and Xiaoyong Chu. Z_2 SIMP Dark Matter. *JCAP*, 1601:006, 2016, 1510.08527.

[62] Jason Pollack, David N. Spergel, and Paul J. Steinhardt. Supermassive Black Holes from Ultra-Strongly Self-Interacting Dark Matter. *Astrophys. J.*, 804(2):131, 2015, 1501.00017.

[63] Samuel B. Roland, Bibhushan Shakya, and James D. Wells. PeV neutrinos and a 3.5 keV x-ray line from a PeV-scale supersymmetric neutrino sector. *Phys. Rev.*, D92(9):095018, 2015, 1506.08195.

[64] Bibhushan Shakya. Sterile Neutrino Dark Matter from Freeze-In. *Mod. Phys. Lett.*, A31(06):1630005, 2016, 1512.02751.

[65] Alexander Merle, Aurel Schneider, and Maximilian Totzauer. Dodelson-Widrow Production of Sterile Neutrino Dark Matter with Non-Trivial Initial Abundance. *JCAP*, 1604(04):003, 2016,

1512.05369.

[66] Johannes König, Alexander Merle, and Maximilian Totzauer. keV Sterile Neutrino Dark Matter from Singlet Scalar Decays: The Most General Case. 2016, 1609.01289.

[67] Raymond T. Co, Francesco D'Eramo, Lawrence J. Hall, and Duccio Pappadopulo. Freeze-In Dark Matter with Displaced Signatures at Colliders. *JCAP*, 1512(12):024, 2015, 1506.07532.

[68] Seyed Yaser Ayazi, S. Mahdi Firouzabadi, and S. Peyman Zakeri. Freeze-in production of Fermionic Dark Matter with Pseudo-scalar and Phenomenological Aspects. *J. Phys.*, G43(9):095006, 2016, 1511.07736.

[69] Matti Heikinheimo and Christian Spethmann. Galactic Centre GeV Photons from Dark Technicolor. *JHEP*, 12:084, 2014, 1410.4842.

[70] John McDonald. Warm Dark Matter via Ultra-Violet Freeze-In: Reheating Temperature and Non-Thermal Distribution for Fermionic Higgs Portal Dark Matter. *JCAP*, 1608(08):035, 2016, 1512.06422.

[71] Esra Bulbul, Maxim Markevitch, Adam Foster, Randall K. Smith, Michael Loewenstein, and Scott W. Randall. Detection of An Unidentified Emission Line in the Stacked X-ray spectrum of Galaxy Clusters. *Astrophys. J.*, 789:13, 2014, 1402.2301.

[72] Alexey Boyarsky, Oleg Ruchayskiy, Dmytro Iakubovskyi, and Jeroen Franse. Unidentified Line in X-Ray Spectra of the Andromeda Galaxy and Perseus Galaxy Cluster. *Phys. Rev. Lett.*, 113:251301, 2014, 1402.4119.

[73] Farinaldo S. Queiroz and Kuver Sinha. The Poker Face of the Majoron Dark Matter Model: LUX to keV Line. *Phys. Lett.*, B735:69–74, 2014, 1404.1400.

[74] Seungwon Baek, P. Ko, and Wan-Il Park. The 3.5 keV X-ray line signature from annihilating and decaying dark matter in Weinberg model. 2014, 1405.3730.

[75] Yasaman Farzan and Amin Rezaei Akbarieh. Decaying Vector Dark Matter as an Explanation for the 3.5 keV Line from Galaxy Clusters. *JCAP*, 1411(11):015, 2014, 1408.2950.

[76] Giorgio Arcadi, Laura Covi, and Federico Dradi. 3.55 keV line in Minimal Decaying Dark Matter scenarios. *JCAP*, 1507(07):023, 2015, 1412.6351.

[77] Alexander Merle and Aurel Schneider. Production of Sterile Neutrino Dark Matter and the 3.5 keV line. *Phys. Lett.*, B749:283–288, 2015, 1409.6311.

[78] Christopher Kolda and James Unwin. X-ray lines from R-parity violating decays of keV sparticles. *Phys. Rev.*, D90:023535, 2014, 1403.5580.

[79] Esra Bulbul, Maxim Markevitch, Adam Foster, Eric Miller, Mark Bautz, Mike Loewenstein, Scott W. Randall, and Randall K. Smith. Searching for the 3.5 keV Line in the Stacked Suzaku Observations of Galaxy Clusters. *Astrophys. J.*, 831(1):55, 2016, 1605.02034.

[80] Felix A. Aharonian et al. Hitomi constraints on the 3.5 keV line in the Perseus galaxy cluster. 2016, 1607.07420.

[81] Joseph P. Conlon, Francesca Day, Nicholas Jennings, Sven Krippendorf, and Markus Rummel. Consistency of Hitomi, XMM-Newton and Chandra 3.5 keV data from Perseus. 2016, 1608.01684.

[82] Maxim Markevitch, A. H. Gonzalez, D. Clowe, A. Vikhlinin, L. David, W. Forman, C. Jones, S. Murray, and W. Tucker. Direct constraints on the dark matter self-interaction cross-section from the merging galaxy cluster 1E0657-56. *Astrophys. J.*, 606:819–824, 2004, astro-ph/0309303.

[83] Scott W. Randall, Maxim Markevitch, Douglas Clowe, Anthony H. Gonzalez, and Marusa Bradac. Constraints on the Self-Interaction Cross-Section of Dark Matter from Numerical Simulations of the Merging Galaxy Cluster 1E 0657-56. *Astrophys. J.*, 679:1173–1180, 2008, 0704.0261.

[84] Miguel Rocha, Annika H. G. Peter, James S. Bullock, Manoj Kaplinghat, Shea Garrison-Kimmel, Jose Onorbe, and Leonidas A. Moustakas. Cosmological Simulations with Self-Interacting Dark Matter I: Constant Density Cores and Substructure. *Mon. Not. Roy. Astron. Soc.*, 430:81–104, 2013, 1208.3025.

[85] Annika H. G. Peter, Miguel Rocha, James S. Bullock, and Manoj Kaplinghat. Cosmological Simulations with Self-Interacting Dark Matter II: Halo Shapes vs. Observations. *Mon. Not. Roy. Astron. Soc.*, 430:105, 2013, 1208.3026.

[86] David Harvey, Richard Massey, Thomas Kitching, Andy Taylor, and Eric Tittley. The non-gravitational interactions of dark matter in colliding galaxy clusters. *Science*, 347:1462–1465, 2015, 1503.07675.

[87] Stacy Y. Kim, Annika H. G. Peter, and David Wittman. In the Wake of Dark Giants: New Signatures of Dark Matter Self Interactions in Equal Mass Mergers of Galaxy Clusters. 2016, 1608.08630.

[88] Richard Massey et al. The behaviour of dark matter associated with four bright cluster galaxies in the 10 kpc core of Abell 3827. *Mon. Not. Roy. Astron. Soc.*, 449(4):3393–3406, 2015, 1504.03388.

[89] Felix Kahlhoefer, Kai Schmidt-Hoberg, Janis Kummer, and Subir Sarkar. On the interpretation of dark matter self-interactions in Abell 3827. *Mon. Not. Roy. Astron. Soc.*, 452(1):L54–L58, 2015, 1504.06576.

[90] Robyn Campbell, Stephen Godfrey, Heather E. Logan, Andrea D. Peterson, and Alexandre Poulin. Implications of the observation of dark matter self-interactions for singlet scalar dark matter. *Phys. Rev.*, D92(5):055031, 2015, 1505.01793.

[91] Ricardo A. Flores and Joel R. Primack. Observational and theoretical constraints on singular dark matter halos. *Astrophys. J.*, 427:L1–4, 1994, astro-ph/9402004.

[92] Julio F. Navarro, Carlos S. Frenk, and Simon D. M. White. A Universal density profile from hierarchical clustering. *Astrophys. J.*, 490:493–508, 1997, astro-ph/9611107.

[93] W. J. G. de Blok. The Core-Cusp Problem. *Adv. Astron.*, 2010:789293, 2010, 0910.3538.

[94] Anatoly A. Klypin, Andrey V. Kravtsov, Octavio Valenzuela, and Francisco Prada. Where are the missing Galactic satellites? *Astrophys. J.*, 522:82–92, 1999, astro-ph/9901240.

[95] Michael Boylan-Kolchin, James S. Bullock, and Manoj Kaplinghat. Too big to fail? The puzzling darkness of massive Milky Way subhaloes. *Mon. Not. Roy. Astron. Soc.*, 415:L40, 2011, 1103.0007.

[96] Kari Enqvist, Sami Nurmi, Tommi Tenkanen, and Kimmo Tuominen. Standard Model with a real singlet scalar and inflation. *JCAP*, 1408:035, 2014, 1407.0659.

[97] Alexander Kusenko, Lauren Pearce, and Louis Yang. Postinflationary Higgs relaxation and the origin of matter-antimatter asymmetry. *Phys. Rev. Lett.*, 114(6):061302, 2015, 1410.0722.

[98] David J. E. Marsh. Axion Cosmology. *Phys. Rept.*, 643:1–79, 2016, 1510.07633.

[99] P. S. Bhupal Dev, Anupam Mazumdar, and Saleh Qutub. Connection between dark matter abundance and primordial tensor perturbations. 2014, 1412.3041.

[100] Mar Bastero-Gil, Rafael Cerezo, and Joao G. Rosa. Inflaton dark matter from incomplete decay. *Phys. Rev.*, D93(10):103531, 2016, 1501.05539.

[101] Tommi Markkanen and Sami Nurmi. Dark matter from gravitational particle production at reheating. 2015, 1512.07288.

[102] N. D. Birrell and P. C. W. Davies. *Quantum Fields in Curved Space*. Cambridge Monographs on Mathematical Physics. Cambridge Univ. Press, Cambridge, UK, 1984.

[103] Alexei A. Starobinsky and Junichi Yokoyama. Equilibrium state of a selfinteracting scalar field in the De Sitter background. *Phys.Rev.*, D50:6357–6368, 1994, astro-ph/9407016.

[104] Matti Herranen, Tommi Markkanen, Sami Nurmi, and Arttu Rajantie. Spacetime curvature and the Higgs stability during inflation. *Phys.Rev.Lett.*, 113(21):211102, 2014, 1407.3141.

[105] Oleg Lebedev. On Stability of the Electroweak Vacuum and the Higgs Portal. *Eur. Phys. J.*, C72:2058, 2012, 1203.0156.

[106] Oleg Lebedev and Alexander Westphal. Metastable Electroweak Vacuum: Implications for Inflation. *Phys. Lett.*, B719:415–418, 2013, 1210.6987.

[107] Kari Enqvist, Rose N. Lerner, Olli Taanila, and Anders Tranberg. Spectator field dynamics in de Sitter and curvaton initial conditions. *JCAP*, 1210:052, 2012, 1205.5446.

[108] Juan C. Bueno Sanchez and Kari Enqvist. On the fate of coupled flat directions during inflation. *JCAP*, 1303:029, 2013, 1210.7007.

[109] Kari Enqvist and Stanislav Rusak. Modulated preheating and isocurvature perturbations. *JCAP*, 1303:017, 2013, 1210.2192.

[110] Taro Kunimitsu and Jun'ichi Yokoyama. Higgs condensation as an unwanted curvaton. *Phys. Rev.*, D86:083541, 2012, 1208.2316.

[111] Kari Enqvist, Tuukka Meriniemi, and Sami Nurmi. Generation of the Higgs Condensate and Its Decay after Inflation. *JCAP*, 1310:057, 2013, 1306.4511.

[112] Kari Enqvist, Sami Nurmi, and Stanislav Rusak. Non-Abelian dynamics in the resonant decay of the Higgs after inflation. *JCAP*, 1410(10):064, 2014, 1404.3631.

[113] Matti Herranen, Tommi Markkanen, Sami Nurmi, and Arttu Rajantie. Spacetime curvature and Higgs stability after inflation. *Phys. Rev. Lett.*, 115:241301, 2015, 1506.04065.

[114] Daniel G. Figueroa, Juan Garcia-Bellido, and Francisco Torrenti. Decay of the standard model Higgs field after inflation. *Phys. Rev.*, D92(8):083511, 2015, 1504.04600.

[115] Kari Enqvist, Sami Nurmi, Stanislav Rusak, and David Weir. Lattice Calculation of the Decay of Primordial Higgs Condensate. *JCAP*, 1602(02):057, 2016, 1506.06895.

[116] Daniel G. Figueroa, Juan García-Bellido, and Francisco Torrentí. Gravitational wave production from the decay of the standard model Higgs field after inflation. *Phys. Rev.*, D93(10):103521, 2016, 1602.03085.

[117] Mikko Laine and Aleksi Vuorinen. Basics of Thermal Field Theory. *Lect. Notes Phys.*, 925:pp.1–281, 2016.

[118] L.F. Abbott, Edward Farhi, and Mark B. Wise. Particle Production in the New Inflationary Cosmology. *Phys.Lett.*, B117:29, 1982.

[119] A. D. Dolgov and Andrei D. Linde. Baryon Asymmetry in Inflationary Universe. *Phys. Lett.*, B116:329, 1982.

[120] Andreas Albrecht, Paul J. Steinhardt, Michael S. Turner, and Frank Wilczek. Reheating an Inflationary Universe. *Phys. Rev. Lett.*, 48:1437, 1982.

[121] Kazuhide Ichikawa, Teruaki Suyama, Tomo Takahashi, and Masahide Yamaguchi. Primordial Curvature Fluctuation and Its Non-Gaussianity in Models with Modulated Reheating. *Phys.Rev.*, D78:063545, 2008, 0807.3988.

[122] Lev Kofman, Andrei D. Linde, and Alexei A. Starobinsky. Reheating after inflation. *Phys. Rev. Lett.*, 73:3195–3198, 1994, hep-th/9405187.

[123] Y. Shtanov, Jennie H. Traschen, and Robert H. Brandenberger. Universe reheating after inflation. *Phys. Rev.*, D51:5438–5455, 1995, hep-ph/9407247.

[124] Lev Kofman, Andrei D. Linde, and Alexei A. Starobinsky. Towards the theory of reheating after inflation. *Phys.Rev.*, D56:3258–3295, 1997, hep-ph/9704452.

[125] Patrick B. Greene, Lev Kofman, Andrei D. Linde, and Alexei A. Starobinsky. Structure of resonance in preheating after inflation. *Phys.Rev.*, D56:6175–6192, 1997, hep-ph/9705347.

[126] Patrick B. Greene and Lev Kofman. Preheating of fermions. *Phys. Lett.*, B448:6–12, 1999, hep-ph/9807339.

[127] G. F. Giudice, M. Peloso, A. Riotto, and I. Tkachev. Production of massive fermions at preheating and leptogenesis. *JHEP*, 08:014, 1999, hep-ph/9905242.

[128] Patrick B. Greene and Lev Kofman. On the theory of fermionic preheating. *Phys. Rev.*, D62:123516, 2000, hep-ph/0003018.

[129] Marco Peloso and Lorenzo Sorbo. Preheating of massive fermions after inflation: Analytical results. *JHEP*, 05:016, 2000, hep-ph/0003045.

[130] Bruce A. Bassett and Stefano Liberati. Geometric reheating after inflation. *Phys. Rev.*, D58:021302, 1998, hep-ph/9709417. [Erratum: Phys. Rev.D60,049902(1999)].

[131] Shinji Tsujikawa, Kei-ichi Maeda, and Takashi Torii. Resonant particle production with non-minimally coupled scalar fields in preheating after inflation. *Phys. Rev.*, D60:063515, 1999, hep-ph/9901306.

[132] Jean Francois Dufaux, Gary N. Felder, L. Kofman, M. Peloso, and D. Podolsky. Preheating with trilinear interactions: Tachyonic resonance. *JCAP*, 0607:006, 2006, hep-ph/0602144.

[133] Andrei Linde. *Particle Physics and Inflationary Cosmology*. Harwood Academic Publisher, 1990, hep-th/0503203.

[134] K. Enqvist and K. J. Eskola. Thermalization in the Early Universe. *Mod. Phys. Lett.*, A5:1919–1926, 1990.

[135] Sacha Davidson and Subir Sarkar. Thermalization after inflation. *JHEP*, 11:012, 2000, hep-ph/0009078.

[136] G.D. Coughlan, W. Fischler, Edward W. Kolb, S. Raby, and Graham G. Ross. Cosmological Problems for the Polonyi Potential. *Phys.Lett.*, B131:59, 1983.

[137] Tom Banks, M. Berkooz, S.H. Shenker, Gregory W. Moore, and P.J. Steinhardt. Modular cosmology. *Phys.Rev.*, D52:3548–3562, 1995, hep-th/9503114.

[138] Tom Banks, M. Berkooz, and P.J. Steinhardt. The Cosmological moduli problem, supersymmetry breaking, and stability in postinflationary cosmology. *Phys.Rev.*, D52:705–716, 1995, hep-th/9501053.

[139] Wayne Hu. Structure formation with generalized dark matter. *Astrophys. J.*, 506:485–494, 1998, astro-ph/9801234.

[140] Wayne Hu, Rennan Barkana, and Andrei Gruzinov. Cold and fuzzy dark matter. *Phys. Rev. Lett.*, 85:1158–1161, 2000, astro-ph/0003365.

[141] Luca Amendola and Riccardo Barbieri. Dark matter from an ultra-light pseudo-Goldsone-boson. *Phys. Lett.*, B642:192–196, 2006, hep-ph/0509257.

[142] David J. E. Marsh and Joe Silk. A Model For Halo Formation With Axion Mixed Dark Matter. *Mon. Not. Roy. Astron. Soc.*, 437(3):2652–2663, 2014, 1307.1705.

[143] Vanda Silveira and A. Zee. Scalar Phantoms. *Phys. Lett.*, B161:136–140, 1985.

[144] John McDonald. Gauge singlet scalars as cold dark matter. *Phys.Rev.*, D50:3637–3649, 1994, hep-ph/0702143.

[145] C. P. Burgess, Maxim Pospelov, and Tonnis ter Veldhuis. The Minimal model of nonbaryonic dark matter: A Singlet scalar. *Nucl. Phys.*, B619:709–728, 2001, hep-ph/0011335.

[146] Brian Patt and Frank Wilczek. Higgs-field portal into hidden sectors. 2006, hep-ph/0605188.

[147] Maxim Pospelov, Adam Ritz, and Mikhail B. Voloshin. Secluded WIMP Dark Matter. *Phys. Lett.*, B662:53–61, 2008, 0711.4866.

[148] Wojciech Krolikowski. A Hidden Valley model of cold dark matter with photonic portal. 2008, 0803.2977.

[149] Yang Bai and Joshua Berger. Lepton Portal Dark Matter. *JHEP*, 08:153, 2014, 1402.6696.

[150] Ankit Beniwal, Filip Rajec, Christopher Savage, Pat Scott, Christoph Weniger, Martin White, and Anthony G. Williams. Combined analysis of effective Higgs portal dark matter models. *Phys. Rev.*, D93(11):115016, 2016, 1512.06458.

[151] Ketevi Assamagan et al. The Higgs Portal and Cosmology. 2016, 1604.05324.

[152] Z. Chacko, Hock-Seng Goh, and Roni Harnik. The Twin Higgs: Natural electroweak breaking from mirror symmetry. *Phys. Rev. Lett.*, 96:231802, 2006, hep-ph/0506256.

[153] Riccardo Barbieri, Thomas Gregoire, and Lawrence J. Hall. Mirror world at the large hadron collider. 2005, hep-ph/0509242.

[154] James M. Cline, Kimmo Kainulainen, Pat Scott, and Christoph Weniger. Update on scalar singlet dark matter. *Phys.Rev.*, D88:055025, 2013, 1306.4710.

[155] Thomas Hambye. Hidden vector dark matter. *JHEP*, 01:028, 2009, 0811.0172.

[156] Joachim Kopp, Jia Liu, Tracy R. Slatyer, Xiao-Ping Wang, and Wei Xue. Impeded Dark Matter. 2016, 1609.02147.

[157] Chris Kouvaris, Ian M. Shoemaker, and Kimmo Tuominen. Self-Interacting Dark Matter through the Higgs Portal. *Phys. Rev.*, D91(4):043519, 2015, 1411.3730.

[158] Alexander Merle, Viviana Niro, and Daniel Schmidt. New Production Mechanism for keV Sterile Neutrino Dark Matter by Decays of Frozen-In Scalars. *JCAP*, 1403:028, 2014, 1306.3996.

[159] Michael Klasen and Carlos E. Yaguna. Warm and cold fermionic dark matter via freeze-in. *JCAP*, 1311:039, 2013, 1309.2777.

[160] K. Rummukainen, M. Tsypin, K. Kajantie, M. Laine, and Mikhail E. Shaposhnikov. The Universality class of the electroweak theory. *Nucl.Phys.*, B532:283–314, 1998, hep-lat/9805013.

[161] Stefano Profumo, Michael J. Ramsey-Musolf, and Gabe Shaughnessy. Singlet Higgs phenomenology and the electroweak phase transition. *JHEP*, 0708:010, 2007, 0705.2425.

[162] James M. Cline and Kimmo Kainulainen. Electroweak baryogenesis and dark matter from a singlet Higgs. *JCAP*, 1301:012, 2013, 1210.4196.

[163] David E. Morrissey and Michael J. Ramsey-Musolf. Electroweak baryogenesis. *New J. Phys.*, 14:125003, 2012, 1206.2942.

[164] Mark Hindmarsh, Stephan J. Huber, Kari Rummukainen, and David J. Weir. Numerical simulations of acoustically generated gravitational waves at a first order phase transition. *Phys. Rev.*, D92(12):123009, 2015, 1504.03291.

[165] Pedro Schwaller. Gravitational Waves from a Dark Phase Transition. *Phys. Rev. Lett.*, 115(18):181101, 2015, 1504.07263.

[166] Pau Amaro Seoane et al. The Gravitational Universe. 2013, 1305.5720.

[167] B. P. Abbott et al. Observation of Gravitational Waves from a Binary Black Hole Merger. *Phys. Rev. Lett.*, 116(6):061102, 2016, 1602.03837.

[168] B. P. Abbott et al. Binary Black Hole Mergers in the first Advanced LIGO Observing Run. *Phys. Rev.*, X6(4):041015, 2016, 1606.04856.

[169] Oleg Lebedev and Hyun Min Lee. Higgs Portal Inflation. *Eur. Phys. J.*, C71:1821, 2011, 1105.2284.

[170] Felix Kahlhoefer and John McDonald. WIMP Dark Matter and Unitarity-Conserving Inflation via a Gauge Singlet Scalar. *JCAP*, 1511(11):015, 2015, 1507.03600.

[171] Tommi Tenkanen. Feebly Interacting Dark Matter Particle as the Inflaton. *JHEP*, 09:049, 2016, 1607.01379.

[172] Kari Enqvist, Daniel G. Figueroa, and Rose N. Lerner. Curvaton Decay by Resonant Production of the Standard Model Higgs. *JCAP*, 1301:040, 2013, 1211.5028.

[173] Kari Enqvist, Rose N. Lerner, and Tomo Takahashi. The minimal curvaton-higgs model. *JCAP*, 1401:006, 2014, 1310.1374.

[174] Tommi Alanne, Kimmo Tuominen, and Ville Vaskonen. Strong phase transition, dark matter and vacuum stability from simple hidden sectors. *Nucl. Phys.*, B889:692–711, 2014, 1407.0688.

[175] Tommi Tenkanen, Kimmo Tuominen, and Ville Vaskonen. A Strong Electroweak Phase Transition from the Inflaton Field. *JCAP*, 1609(09):037, 2016, 1606.06063.

[176] J.R. Espinosa, G.F. Giudice, and A. Riotto. Cosmological implications of the Higgs mass measurement. *JCAP*, 0805:002, 2008, 0710.2484.

[177] Joan Elias-Miro, Jose R. Espinosa, Gian F. Giudice, Gino Isidori, Antonio Riotto, and Alessandro Strumia. Higgs mass implications on the stability of the electroweak vacuum. *Phys. Lett.*, B709:222–228, 2012, 1112.3022.

[178] Matthew Gonderinger, Yingchuan Li, Hiren Patel, and Michael J. Ramsey-Musolf. Vacuum Stability, Perturbativity, and Scalar Singlet Dark Matter. *JHEP*, 01:053, 2010, 0910.3167.

[179] Joan Elias-Miro, Jose R. Espinosa, Gian F. Giudice, Hyun Min Lee, and Alessandro Strumia. Stabilization of the Electroweak Vacuum by a Scalar Threshold Effect. *JHEP*, 06:031, 2012, 1203.0237.

[180] Wei Chao, Matthew Gonderinger, and Michael J. Ramsey-Musolf. Higgs Vacuum Stability, Neutrino Mass, and Dark Matter. *Phys. Rev.*, D86:113017, 2012, 1210.0491.

[181] Archil Kobakhidze and Alexander Spencer-Smith. Electroweak Vacuum (In)Stability in an Inflationary Universe. *Phys.Lett.*, B722:130–134, 2013, 1301.2846.

[182] Malcolm Fairbairn and Robert Hogan. Electroweak Vacuum Stability in light of BICEP2. *Phys.Rev.Lett.*, 112:201801, 2014, 1403.6786.

[183] Anson Hook, John Kearney, Bibhushan Shakya, and Kathryn M. Zurek. Probable or Improbable Universe? Correlating Electroweak Vacuum Instability with the Scale of Inflation. *JHEP*, 1501:061, 2015, 1404.5953.

[184] Ian G. Moss. Vacuum stability and the scaling behaviour of the Higgs-curvature coupling. 2015, 1509.03554.

[185] Jose R. Espinosa, Gian F. Giudice, Enrico Morgante, Antonio Riotto, Leonardo Senatore, Alessandro Strumia, and Nikolaos Tetradis. The cosmological Higgstory of the vacuum instability. *JHEP*, 09:174, 2015, 1505.04825.

[186] Kfir Blum, Raffaele Tito D'Agnolo, and JiJi Fan. Vacuum stability bounds on Higgs coupling deviations in the absence of new bosons. *JHEP*, 03:166, 2015, 1502.01045.

[187] Michela D'Onofrio, Kari Rummukainen, and Anders Tranberg. Sphaleron Rate in the Minimal Standard Model. *Phys. Rev. Lett.*, 113(14):141602, 2014, 1404.3565.

[188] Andrey Katz and Maxim Perelstein. Higgs Couplings and Electroweak Phase Transition. *JHEP*, 07:108, 2014, 1401.1827.

[189] Vardan Khachatryan et al. Precise determination of the mass of the Higgs boson and tests of compatibility of its couplings with the standard model predictions using proton collisions at 7 and 8 TeV. *Eur. Phys. J.*, C75(5):212, 2015, 1412.8662.

[190] Georges Aad et al. Measurements of the Higgs boson production and decay rates and coupling strengths using pp collision data at $\sqrt{s} = 7$ and 8 TeV in the ATLAS experiment. *Eur. Phys. J.*, C76(1):6, 2016, 1507.04548.

[191] D. S. Akerib et al. Improved Limits on Scattering of Weakly Interacting Massive Particles from Reanalysis of 2013 LUX Data. *Phys. Rev. Lett.*, 116(16):161301, 2016, 1512.03506.

[192] Daniel J. H. Chung and Hojin Yoo. Isocurvature Perturbations and Non-Gaussianity of Gravitationally Produced Nonthermal Dark Matter. *Phys. Rev.*, D87:023516, 2013, 1110.5931.

[193] Daniel J. H. Chung, Hojin Yoo, and Peng Zhou. Fermionic Isocurvature Perturbations. *Phys. Rev.*, D91(4):043516, 2015, 1306.1966.

[194] Matteo Viel, George D. Becker, James S. Bolton, and Martin G. Haehnelt. Warm dark matter as a solution to the small scale crisis: New constraints from high redshift Lyman-alpha forest data. *Phys. Rev.*, D88:043502, 2013, 1306.2314.

[195] Marcelo Alvarez et al. Testing Inflation with Large Scale Structure: Connecting Hopes with Reality. 2014, 1412.4671.

[196] Francis-Yan Cyr-Racine, Kris Sigurdson, Jesus Zavala, Torsten Bringmann, Mark Vogelsberger, and Christoph Pfrommer. ETHOS—an effective theory of structure formation: From dark

particle physics to the matter distribution of the Universe. *Phys. Rev.*, D93(12):123527, 2016, 1512.05344.

[197] A. Kogut et al. The Primordial Inflation Explorer (PIXIE): A Nulling Polarimeter for Cosmic Microwave Background Observations. *JCAP*, 1107:025, 2011, 1105.2044.

[198] T. Matsumura et al. Mission design of LiteBIRD. 2013, 1311.2847. [J. Low. Temp. Phys.176,733(2014)].

[199] Luca Amendola et al. Cosmology and Fundamental Physics with the Euclid Satellite. 2016, 1606.00180.